外场调控下二维

Dirac 电子的量子输运

金国钧

2015.6.11

一. 引言

Emergence of graphene

Electric Field Effect in Atomically Thin Carbon Films

Novoselov et al., **Science 306, 666 (2004)**

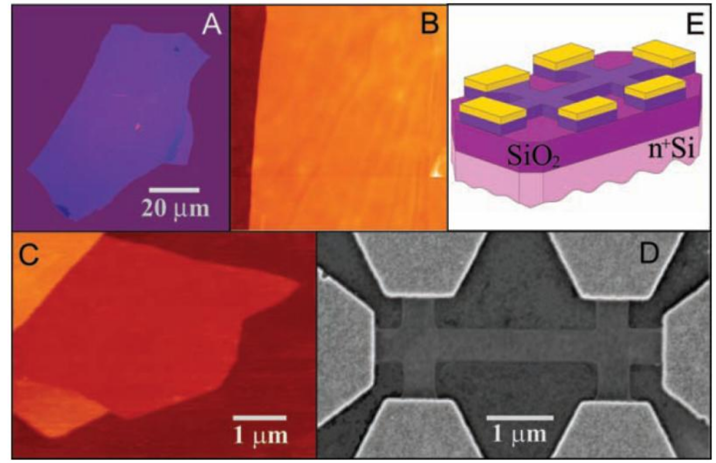

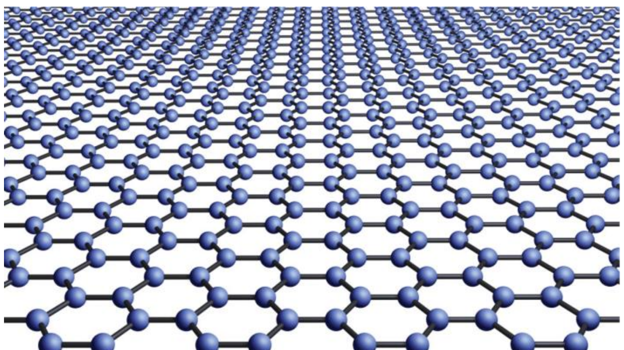

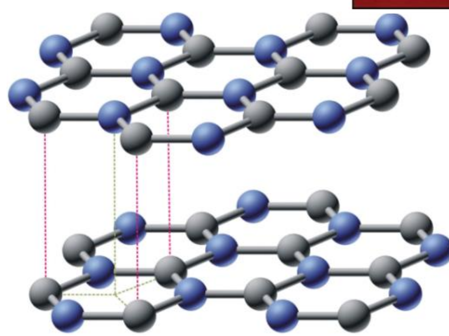

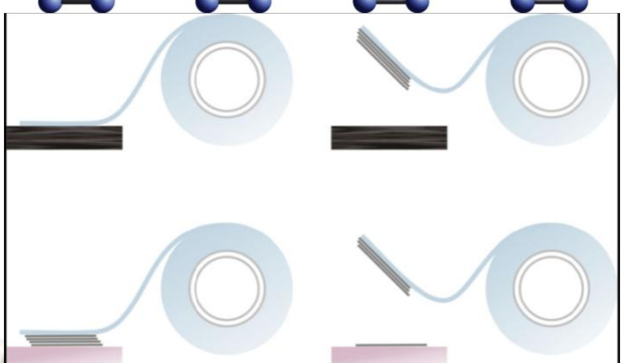

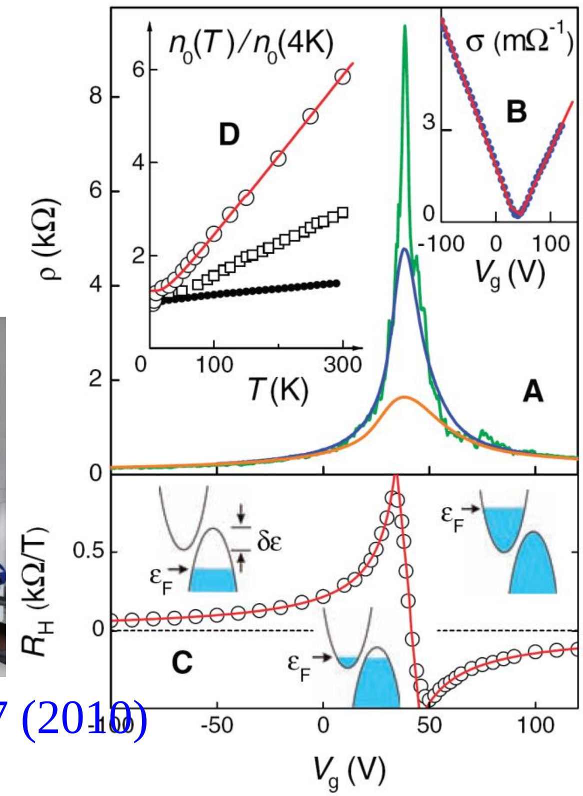

Graphene: Materials in the Flatland Novoselov, RMP 83, 837 (2010)

Carbon Wonderland

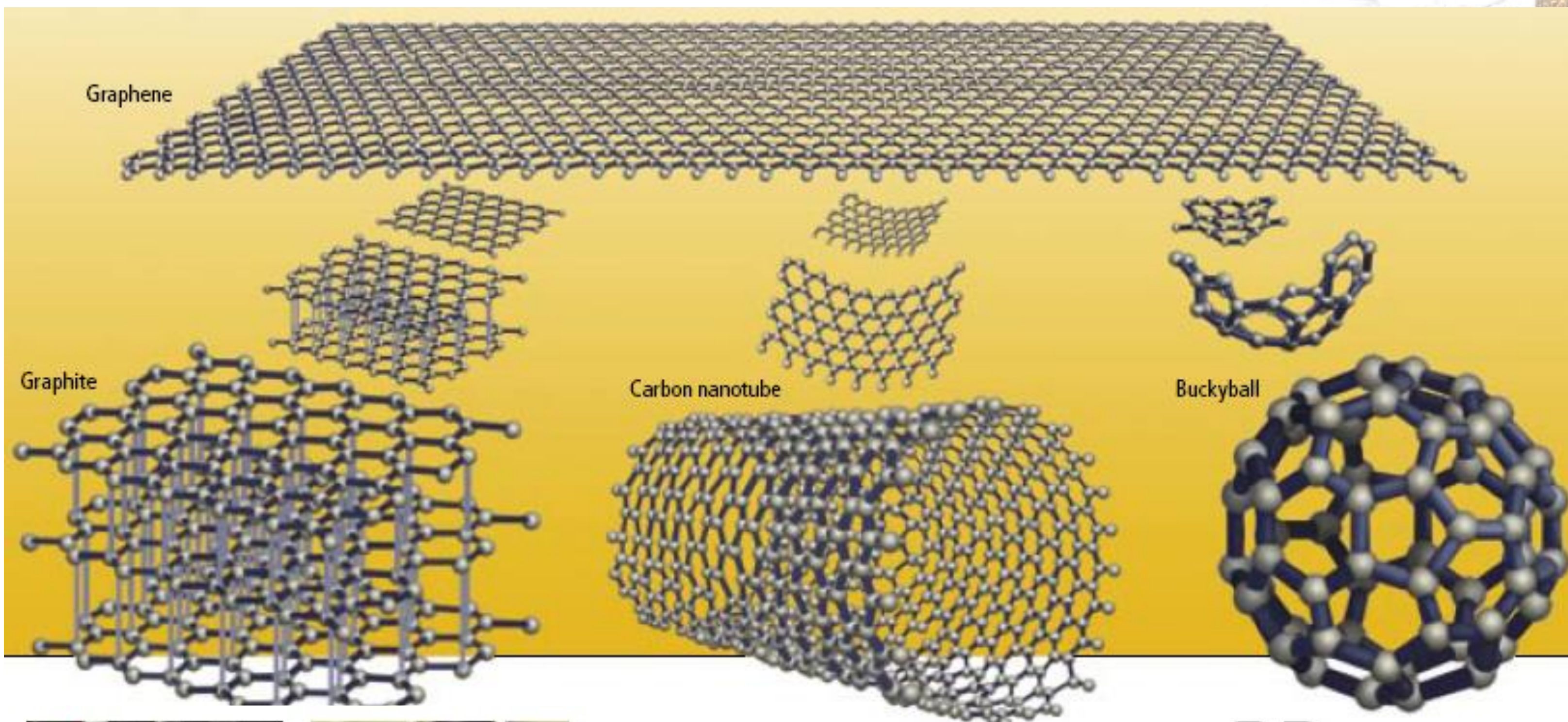

Geim(Manchester)

Kim (Columbia)

A. K. Geim and P. Kim,
Sci. Am. April, 90 (2008)

3D

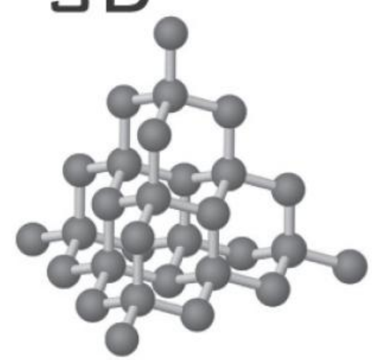

明星材料—碳单层

Ultrathin Epitaxial Graphite: …

C. Berger et al., J. Phys. Chem. B 108, 19912 (2004)

凝聚态物理学中的相对论效应！ Geim and MacDonald, Phys. Today, Aug. 35 (2007)

Graphene: Exploring carbon flatland

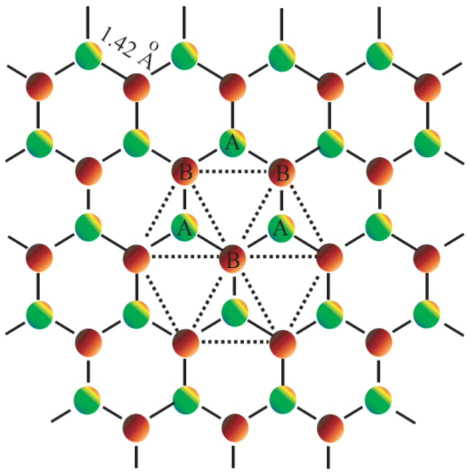

(a)

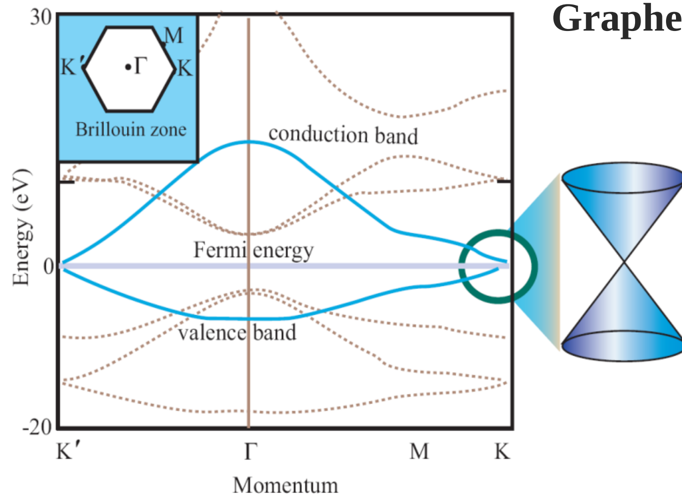

(b)

无质量 Dirac Fermi 子

$$\mathcal{H} = v_{\mathrm{F}}\, p \begin{pmatrix} 0 & e^{i\varphi(p)} \\ e^{-i\varphi(p)} & 0 \end{pmatrix}$$

有质量普通自由粒子

$$\mathcal{H} = \frac{p^2}{2m}$$

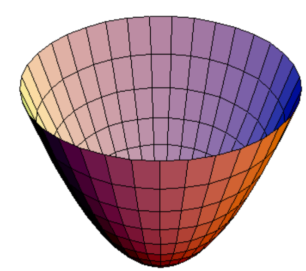

异常量子Hall效应

Novoselov et al.,

Nature **438**, 197 (2005)

$$E_N = \mathrm{sgn}(N)\sqrt{2e\hbar v_{\mathrm{F}}^2 \,|\, N \,|\, B}$$

$$\sigma_{xy} = \pm 4(N+1/2)e^2/h$$

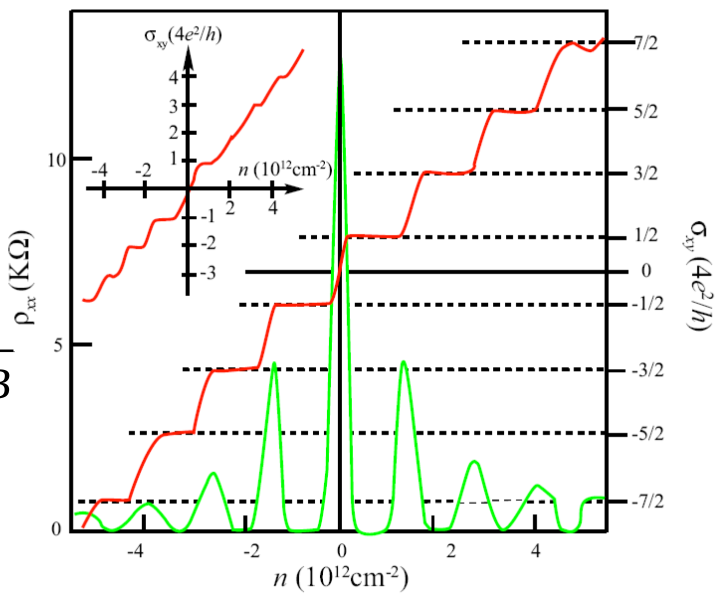

二. 电偏压诱导下

碳双层结构中的激子凝聚

和热 *Josephson* 效应

C. Zhang and G. Jin, JPCM **25**, 425604 (2013).

C. Zhang and G. Jin, APL **103**, 202111 (2013).

1. Background: Physical picture of excitons

a quasiparticle = an electron in conduction band
+ a hole in valence band with Coulomb interaction

$$\left[-\frac{\hbar^2\nabla_{\mathrm{e}}^2}{2m_{\mathrm{e}}}-\frac{\hbar^2\nabla_{\mathrm{h}}^2}{2m_{\mathrm{h}}}-\frac{e^2}{\epsilon|\boldsymbol{r}_{\mathrm{e}}-\boldsymbol{r}_{\mathrm{h}}|}\right]\Phi(\boldsymbol{r}_{\mathrm{e}},\boldsymbol{r}_{\mathrm{h}})=E\Phi(\boldsymbol{r}_{\mathrm{e}},\boldsymbol{r}_{\mathrm{h}})$$

play important role in the optical properties of semiconductors

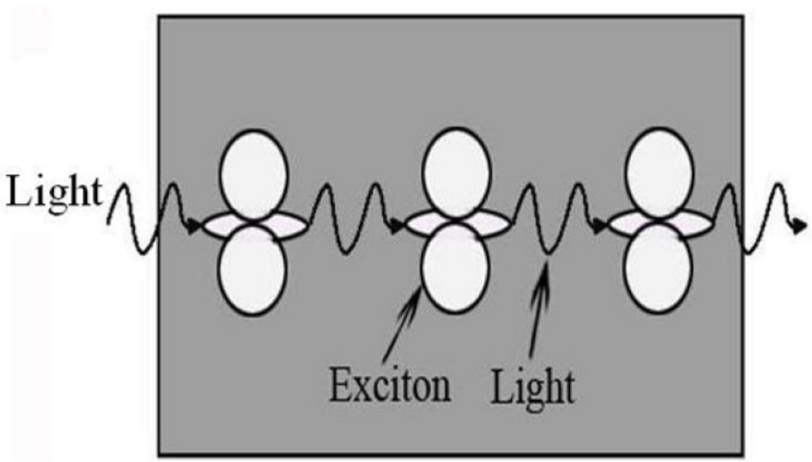

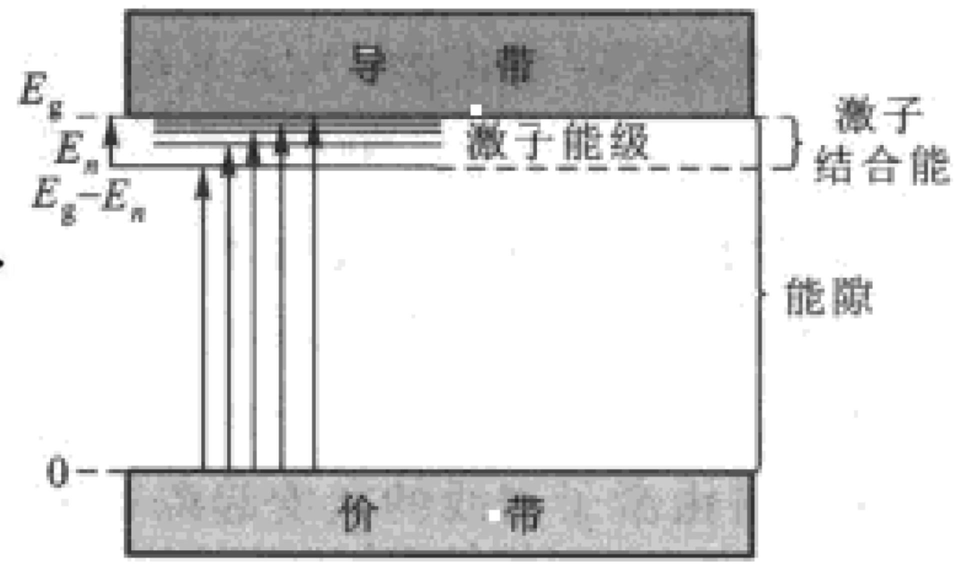

At low density, excitons as bosons → Bose condensation

1. Background: Exciton condensation

proposed by Keldysh and Kopaev in1964 and studied by Soviet physicists

L. V. Keldysh and Y. V. Kopaev, Fiz. Tverd. Tela 6, 2791 (1964)

since then a lot of experiments on this subject

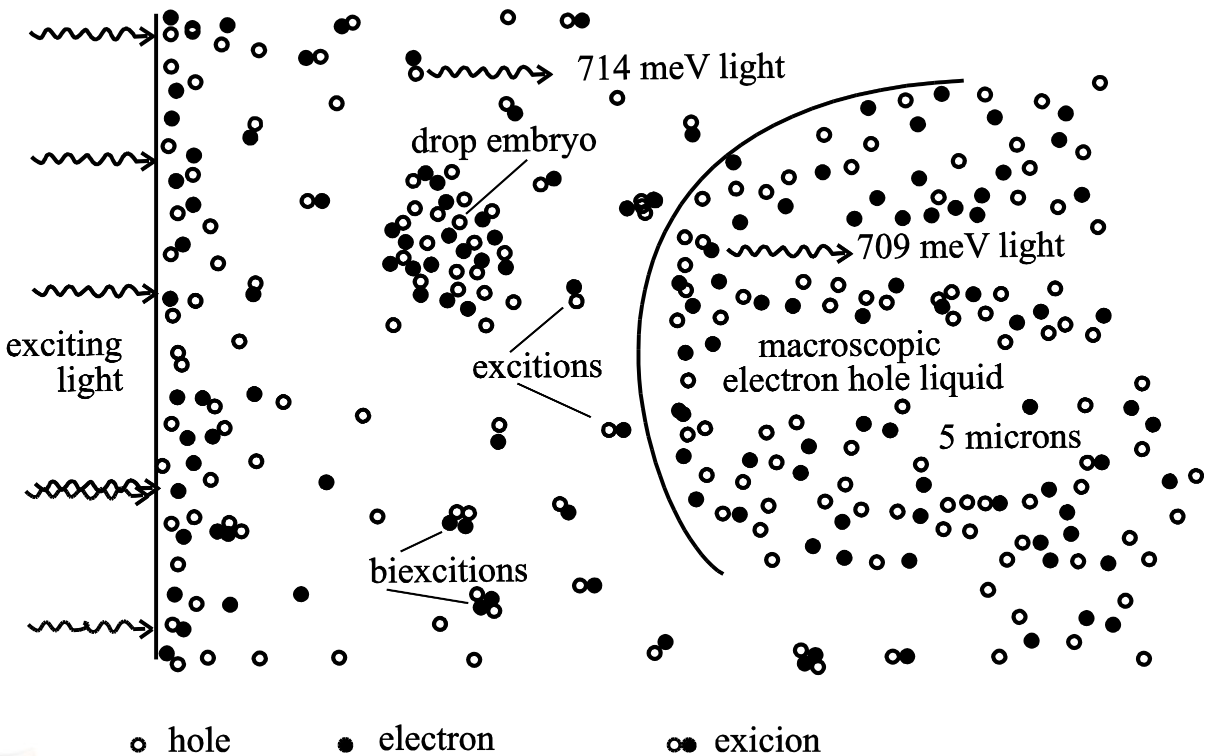

experiment on Ge crystal luminescence

Electron-Hole Condensation in Semiconductors, C. D. Jeffries, Science **189**, 955 (1975)

still no direct evidence due to lack of interference

1. Background：Excitons in double quantum wells

LETTER Nature **483**, 584 (2012)
doi:10.1038/nature10903

Spontaneous coherence in a cold exciton gas

A. A. High[1], J. R. Leonard[1], A. T. Hammack[1], M. M. Fogler[1], L. V. Butov[1], A. V. Kavokin[2,3], K. L. Campman[4] & A. C. Gossard[4]

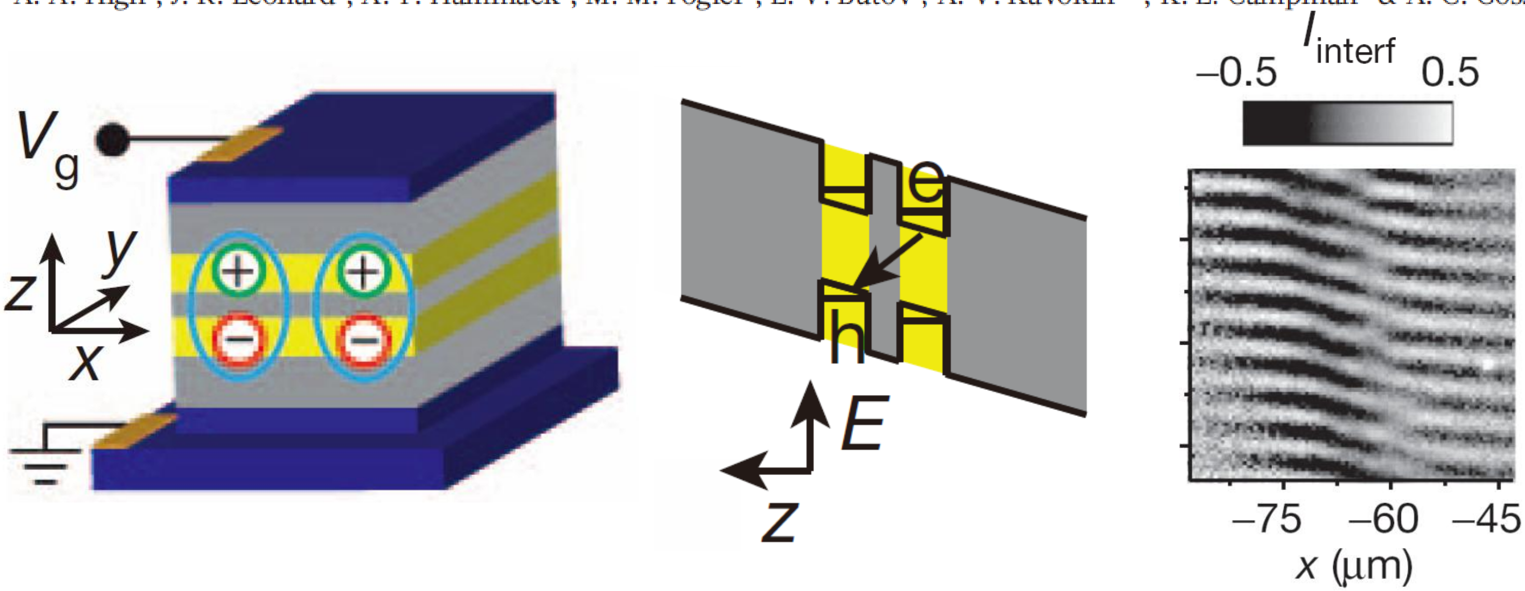

自发相干性是动量空间凝聚的关键特征

通过近几年的研究工作，双量子阱中的激子凝聚现象有了实验依据。特别是，**Graphene** 和拓扑绝缘体的出现，激子凝聚现象又热了起来

2. Exciton condensation in graphene bilayer:

Previousur research

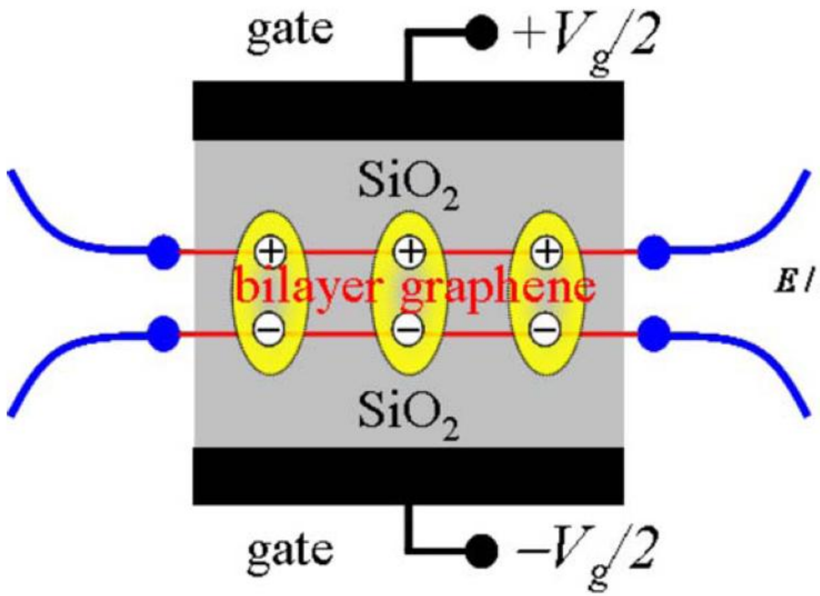

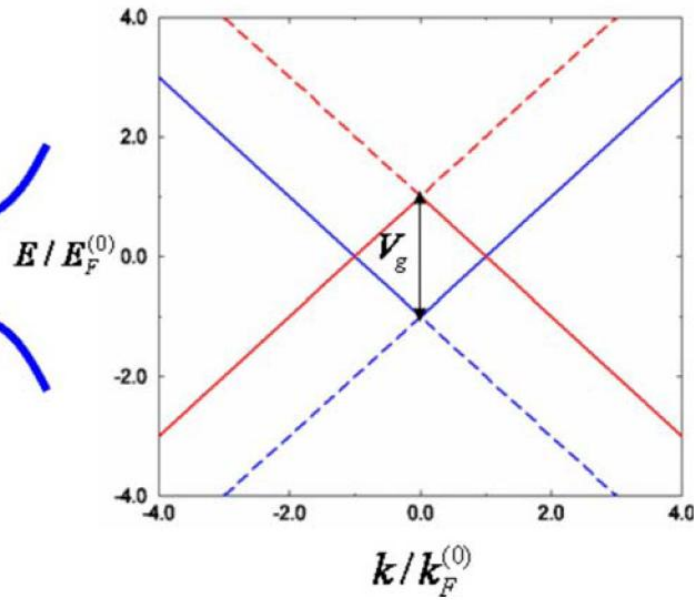

这种结构中无质量 **Fermi** 子 的激子色散关系，凝聚及相关的性质

C.-H. Zhang and Y. N. Joglekar, PRB **77**, 233405 (2008)

H. Min, R. Bistritzer, J. J. Su, and A. H. MacDonald, PRB **78**, 121401(R) (2008)

indicate possible room-temperature superfluidity

2. Exciton condensation in graphene bilayer:

Our considerations

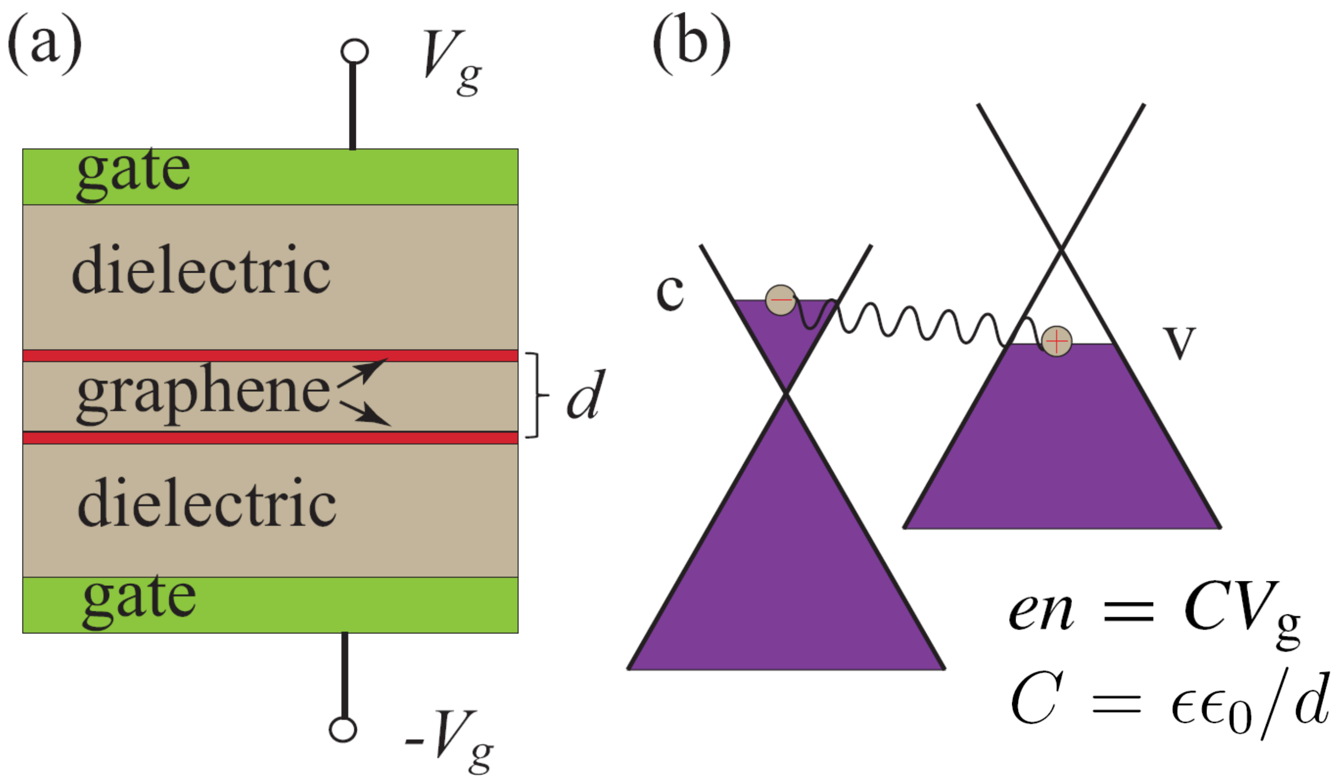

(a）中间有电介质插层的碳双层. 外加的电压可以调节每一碳单层中粒子浓度. (b）两个碳单层的 Fermi 面，分别处在导带 c 和价带 v 上

2. Exciton condensation in graphene bilayer:

Formulation

$$\mathcal{H} = \sum_{\boldsymbol{k}} \left[(\hbar v_{\mathrm{F}} k - eV_{\mathrm{g}}) a^{\dagger}_{\mathrm{c}\boldsymbol{k}} a_{\mathrm{c}\boldsymbol{k}} + (-\hbar v_{\mathrm{F}} k + eV_{\mathrm{g}}) a^{\dagger}_{\mathrm{v}\boldsymbol{k}} a_{\mathrm{v}\boldsymbol{k}} \right]$$
$$+ \frac{1}{2} \sum_{\boldsymbol{k}\boldsymbol{k}'\boldsymbol{q}} [U^{\mathrm{ee}}_{\boldsymbol{q}} a^{\dagger}_{\mathrm{c},\boldsymbol{k}+\boldsymbol{q}} a^{\dagger}_{\mathrm{c},\boldsymbol{k}'-\boldsymbol{q}} a_{\mathrm{c}\boldsymbol{k}'} a_{\mathrm{c}\boldsymbol{k}} + U^{\mathrm{hh}}_{\boldsymbol{q}} a_{\mathrm{v},\boldsymbol{k}+\boldsymbol{q}}$$
$$\times a_{\mathrm{v},\boldsymbol{k}'-\boldsymbol{q}} a^{\dagger}_{\mathrm{v}\boldsymbol{k}'} a^{\dagger}_{\mathrm{v}\boldsymbol{k}} - 2U^{\mathrm{eh}}_{\boldsymbol{q}} a^{\dagger}_{\mathrm{c},\boldsymbol{k}+\boldsymbol{q}} a_{\mathrm{v},\boldsymbol{k}'-\boldsymbol{q}} a^{\dagger}_{\mathrm{v}\boldsymbol{k}'} a_{\mathrm{c}\boldsymbol{k}}]$$

Mean field treatment ← BCS like theory

Broken symmetry → condensed phase to appear

2. Exciton condensation in graphene bilayer:

A set of coupled equations

$$E_{+}(k) = \hbar v_{\mathrm{F}} k - eV_{\mathrm{g}} + \frac{2\pi e^{2} n d}{\epsilon} - \sum_{k'} U^{\mathrm{ee}}_{\boldsymbol{k}'-\boldsymbol{k}} [|v_{k'}|^{2} + (|u_{k'}|^{2} - |v_{k'}|^{2}) f(\varepsilon(k'))],$$

$$\Delta(k) = \frac{1}{2} \sum_{\boldsymbol{k}'} U^{\mathrm{eh}}_{\boldsymbol{k}'-\boldsymbol{k}} \frac{\Delta(k')}{\varepsilon(k')} \left[1 - 2f(\varepsilon(k'))\right],$$

$$\varepsilon(k) = \sqrt{E_{+}(k)^{2} + \Delta(k)^{2}},$$

$$n = 4\sum_{k} \left[|v_{k}|^{2} + (|u_{k}|^{2} - |v_{k}|^{2}) f(\varepsilon(k))\right],$$

$$|v_{k}|^{2} = 1 - |u_{k}|^{2} = [1 - E_{+}(k)/\varepsilon(k)]/2$$

They could be solved self-consistently

2. Exciton condensation in graphene bilayer:

Condensation at zero temperature

$$\beta = e^2/(\epsilon\hbar v_F)$$

$$r_s = 1/\sqrt{\pi n}$$

基态保真度

$$\chi(V_g) = \frac{1}{2\pi}\int\left[\left(\frac{du_k}{dV_g}\right)^2 + \left(\frac{dv_k}{dV_g}\right)^2\right] k\,dk$$

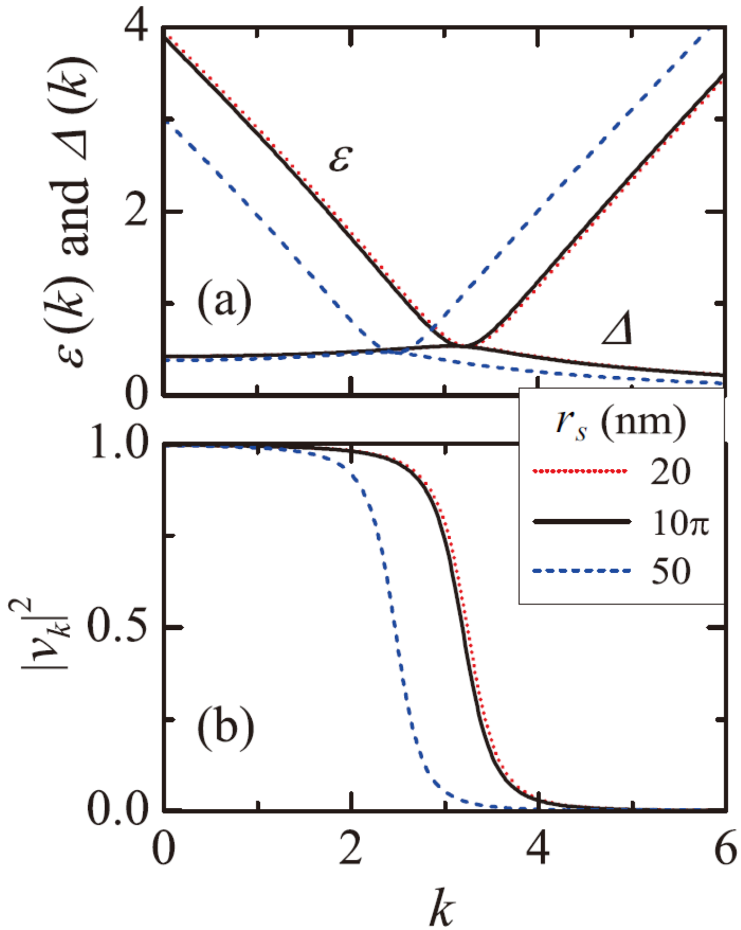

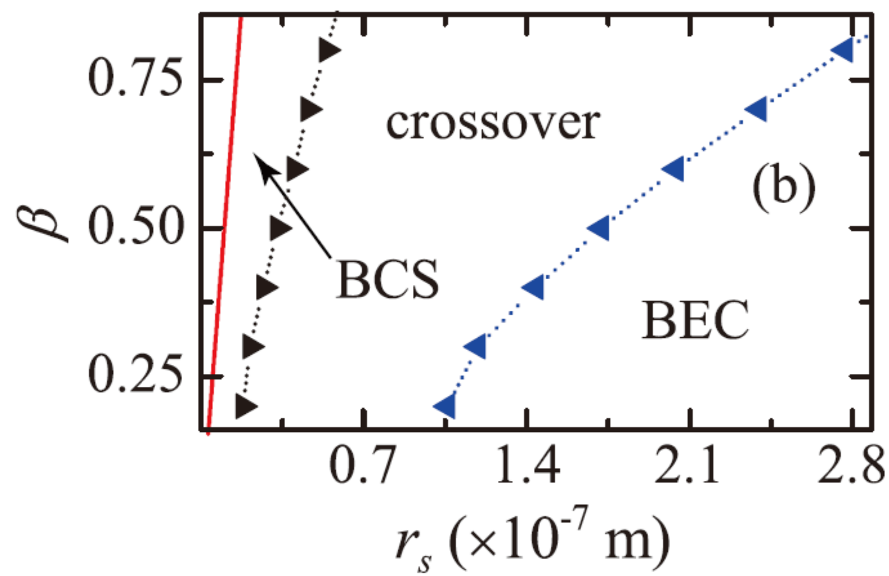

$$k_m \approx \frac{1-2d\beta/r_s}{r_s k_u(1-2\beta/\pi)}$$ 凝聚条件 $\frac{d}{r_s} < \frac{1}{2\beta}$

碳双层中凝聚的相图，它准确地区分激子的BEC态、BCS态及其交叠区域

2. Exciton condensation in graphene bilayer:

Superfluidity at finite temperature $(0 < T < T_C)$

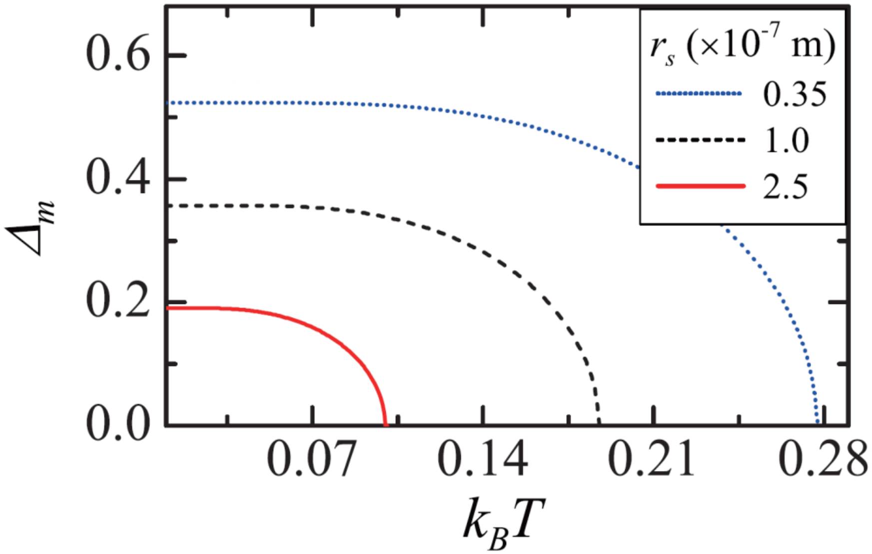

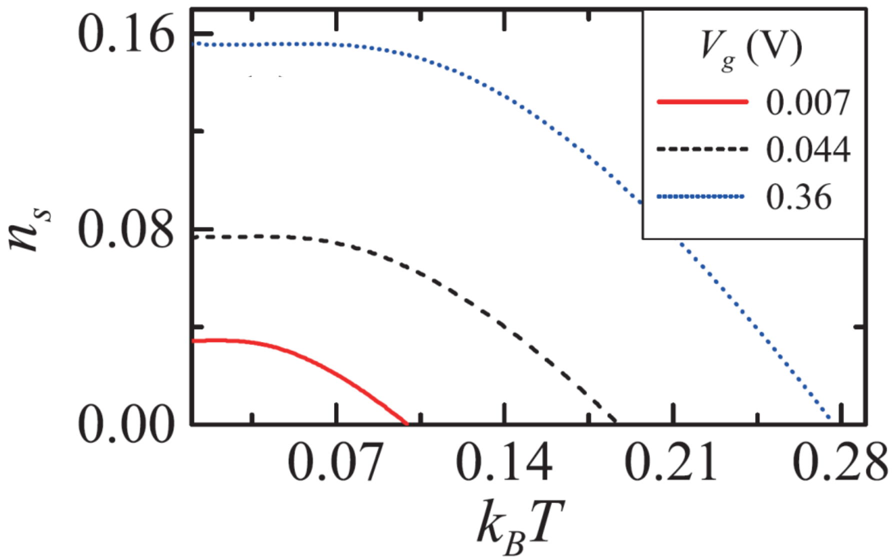

$\Delta_m(0)/(k_B T_c) \approx 1.76$ as for conventional superconductor

$$n_s \approx \frac{\hbar^2 v_F^2}{16\pi k_B T} \int \left(\mathrm{sech}^2 \frac{E_+(k)}{2k_B T} - \mathrm{sech}^2 \frac{\varepsilon(k)}{2k_B T} \right) k \, dk$$

3. Thermal Josephson effect in graphene bilayer:

Previous studies K. Maki and A. Griffin, PRL **15**, 921 (1965) Entropy transport between two superconductors by electron tunneling,

LETTER Nature **492**, 401 (2012)

doi:10.1038/nature11702

The Josephson heat interferometer

Francesco Giazotto[1] & María José Martínez-Pérez[1]

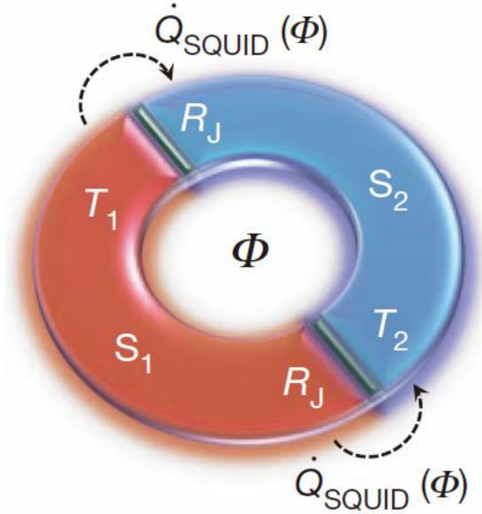

$$\dot{Q}_{SQUID}(\Phi) = 2\dot{Q}_{qp} - 2\dot{Q}_{int}\left|\cos\left(\frac{\pi\Phi}{\Phi_0}\right)\right|$$

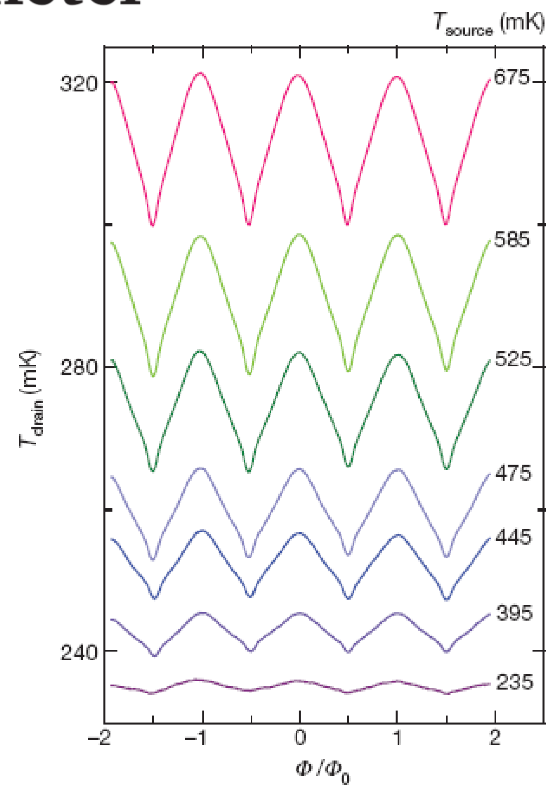

phase-dependent thermal transport

3. Thermal Josephson effect in graphene bilayers:

Our considerations

assume $T_L \geq T_R$

Josephson (1940-)

直流 Josephson 效应

$$I = I_c \sin \Delta\phi$$

交流 Josephson 效应

$$I(t) = I_c \sin(2eVt/\hbar)$$

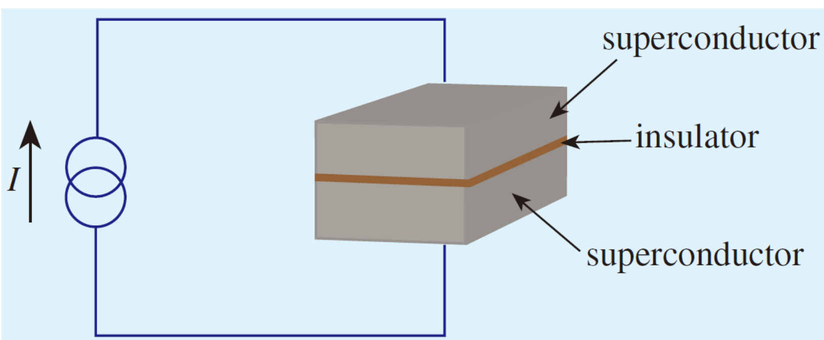

B. D. Josephson, Phys. Lett. **1**, 251 (1962)

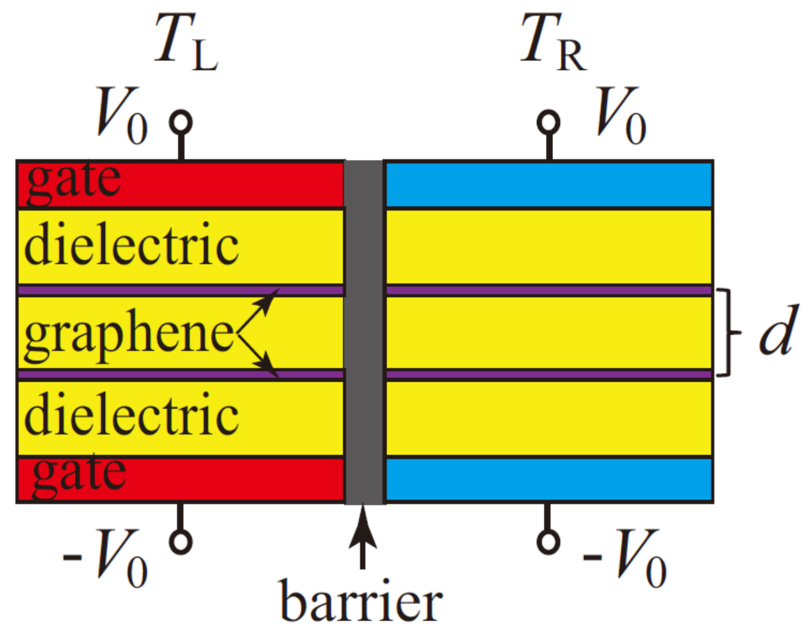

温度偏置的激子凝聚体 Josephson 结示意图. 在绝缘层的每一边，两个碳单层间用厚度为 d 的介电层隔开

3. Thermal Josephson effect in graphene bilayers:

Formulation

ignore the intra-plane interactions

$$\mathcal{H} = \sum_{j\boldsymbol{k}} \left[(\hbar v_{\mathrm{F}} k - V_0) a^{\dagger}_{j\mathrm{c}\boldsymbol{k}} a_{j\mathrm{c}\boldsymbol{k}} + (-\hbar v_{\mathrm{F}} k + V_0) a^{\dagger}_{j\mathrm{v}\boldsymbol{k}} a_{j\mathrm{v}\boldsymbol{k}} \right] - \sum_{j\boldsymbol{k}\boldsymbol{k}'\boldsymbol{q}} U_{\boldsymbol{q}} a^{\dagger}_{j\mathrm{c}\boldsymbol{k}+\boldsymbol{q}} a_{j\mathrm{v}\boldsymbol{k}'-\boldsymbol{q}} a^{\dagger}_{j\mathrm{v}\boldsymbol{k}'} a_{j\mathrm{c}\boldsymbol{k}} + \sum_{\boldsymbol{k}\boldsymbol{k}'} \Gamma_{\boldsymbol{k}\boldsymbol{k}'} \left(a^{\dagger}_{\mathrm{Lc}\boldsymbol{k}} a_{\mathrm{Rc}\boldsymbol{k}'} + a^{\dagger}_{\mathrm{Lv}\boldsymbol{k}} a_{\mathrm{Rv}\boldsymbol{k}'} + a^{\dagger}_{\mathrm{Rc}\boldsymbol{k}'} a_{\mathrm{Lc}\boldsymbol{k}} + a^{\dagger}_{\mathrm{Rv}\boldsymbol{k}'} a_{\mathrm{Lv}\boldsymbol{k}} \right)$$

but add the inter-bilayer tunneling

By using equation of motion, thermal current is

$$I_{\mathrm{Q}} = I_{\mathrm{qp}} + I_{\mathrm{in}}$$

$\pm$ represents $\hbar v_{\mathrm{F}} k \geq V_0$ and the other

$$I_{\mathrm{qp}} = \frac{32|\Gamma|^2}{\pi(\hbar v_{\mathrm{F}})^2} \int_0^{+\infty} (V_0 \pm \sqrt{\varepsilon^2 - \Delta_{\mathrm{L}}^2}) \left[f_{\mathrm{L}}(\varepsilon) - f_{\mathrm{R}}(\varepsilon) \right] \frac{\varepsilon^2}{\sqrt{\varepsilon^2 - \Delta_{\mathrm{L}}^2}} k dk$$

$$I_{\mathrm{in}} = -\frac{32|\Gamma|^2}{\pi(\hbar v_{\mathrm{F}})^2} \cos\varphi \int_0^{+\infty} (V_0 \pm \sqrt{\varepsilon^2 - \Delta_{\mathrm{L}}^2}) \left[f_{\mathrm{L}}(\varepsilon) - f_{\mathrm{R}}(\varepsilon) \right] \frac{\Delta_{\mathrm{L}} \Delta_{\mathrm{R}}}{\sqrt{\varepsilon^2 - \Delta_{\mathrm{L}}^2}} k dk$$

3. Thermal Josephson effect in graphene bilayers:

Transport

两边温度都很低时，$I_Q \approx \frac{16\pi|\Gamma|^2 k_B^2 T_R (T_L - T_R)}{3(\hbar v_F r)^2}$ (for φ =0)

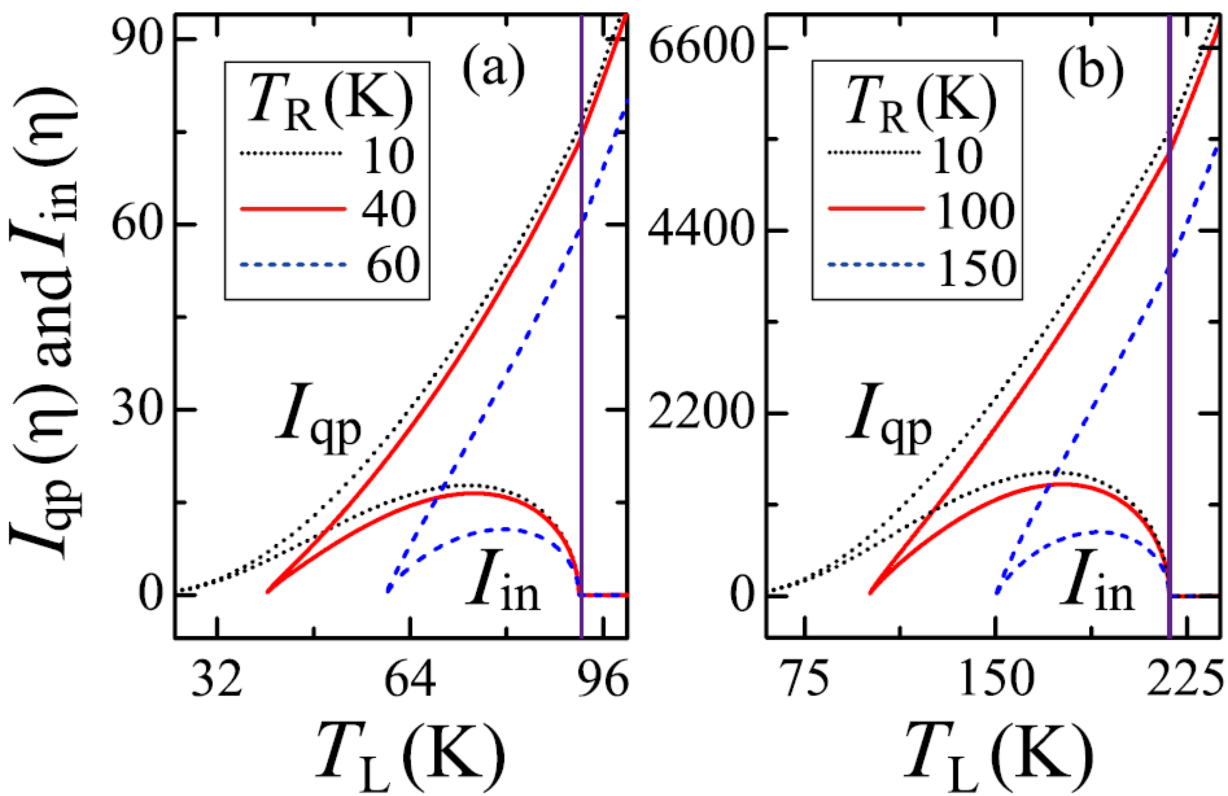

热流 I_{qp} 和 I_{in} 随左边激子凝聚体温度 T_L 的变化．在(a)和(b)中 r 分别为 20 nm 和 5 nm

3. Thermal Josephson effect in graphene bilayers:

Thermal rectification

$$\kappa = \frac{I_{\mathrm{LR}} - I_{\mathrm{RL}}}{I_{\mathrm{RL}}}$$

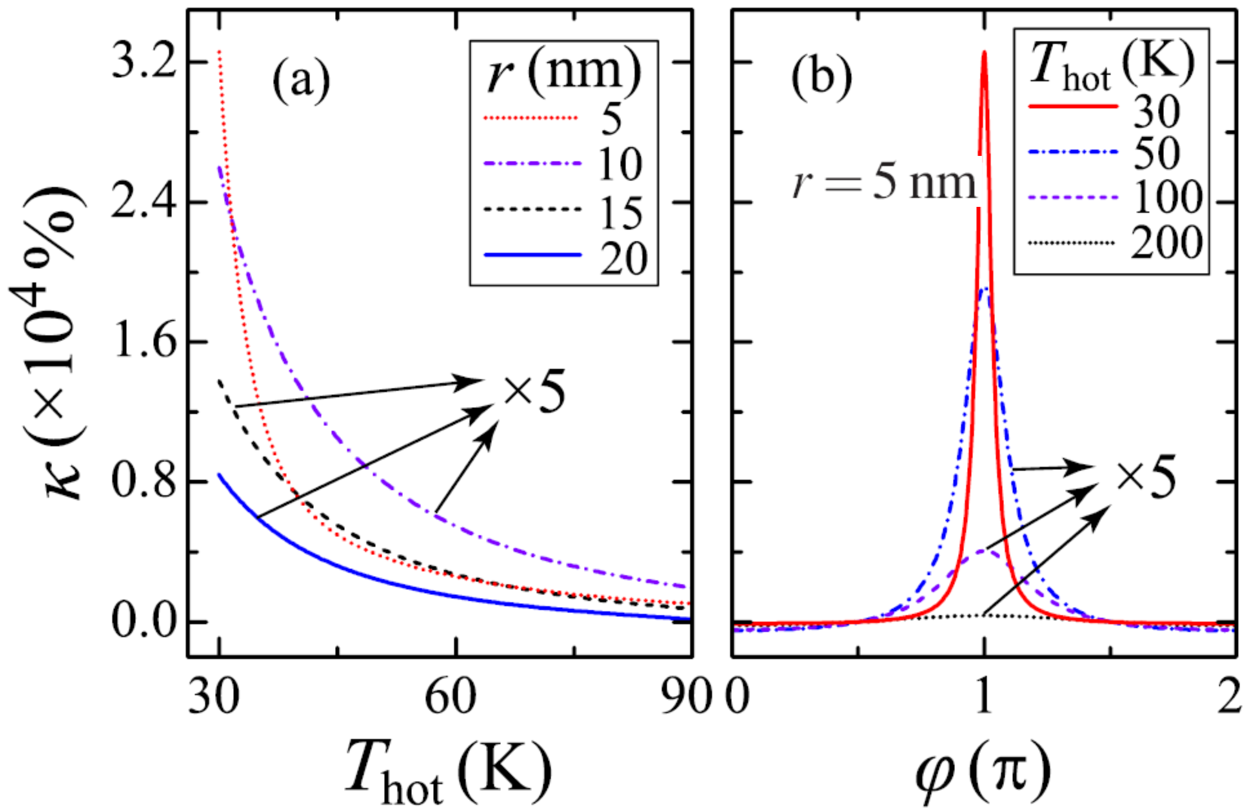

在两个凝聚体**相位差为π**时，整流效果最好，热整流比能达到 **3.3 ×10⁴ %**

热整流比κ 随温度 T_{hot}（a）和相位差（b）的变化，取 T_{cold}=20 K

3. Thermal Josephson effect in graphene bilayers:

Thermal logic gate $T_{\mathrm{L}} = (80 - 70\cos\alpha)\ \mathrm{K}$

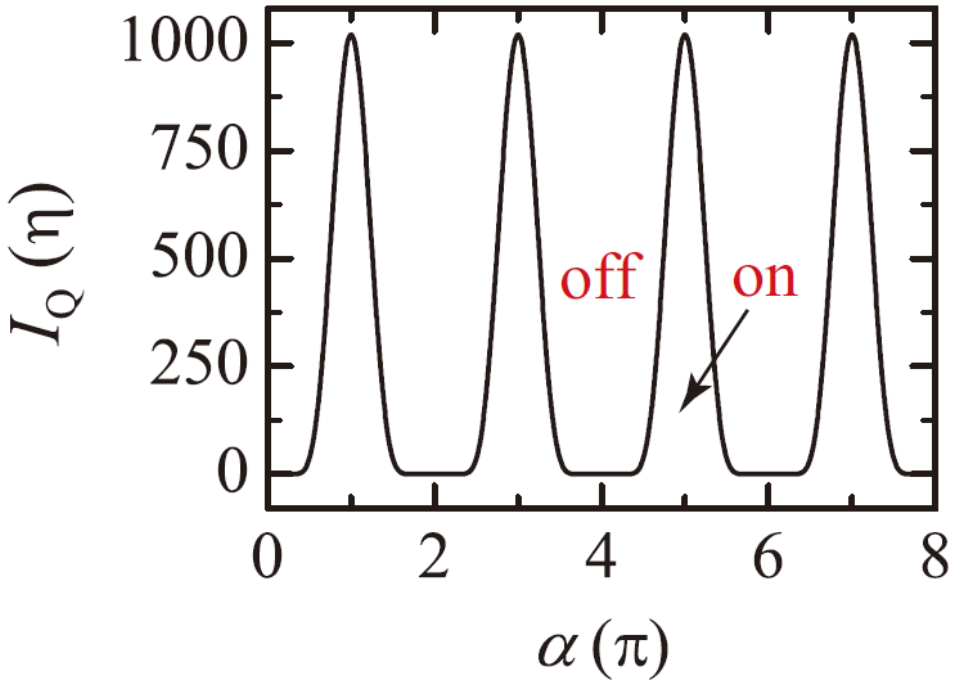

实现**热逻辑门**，很容易通过参数调节获得 on 与 off 态

总热流 I_Q 随参数 α 的变化. 取 T_R=10 K 及 r = 5 nm

4. Summary: Some conclusions

For the exciton condensation in graphene bilayer and thermal Josephson effect in two coupled graphene bilayers, interesting results are

1) derived the criterion of criticality for exciton condensation;

2) obtained the phase diagram to distinguish BEC and BCS states;

3) investigated the thermal transport through a Josephson junction;

4) proposed physically two thermally controllable devices

三. 层间偏压调制下

硼氮双层中的

拓扑量子相变

X. Zhai and G. Jin, APL **102**, 023104 (2013).

X. Zhai and G. Jin, Spin **03**, 1330006 (2013).

X. Zhai and G. Jin, JPCM **26**, 015304 (2014).

1. Background: Graphene mono- and multi-layers

C. L. Kane and E. J. Mele, PRL 95, 226801, 146802 (2005).

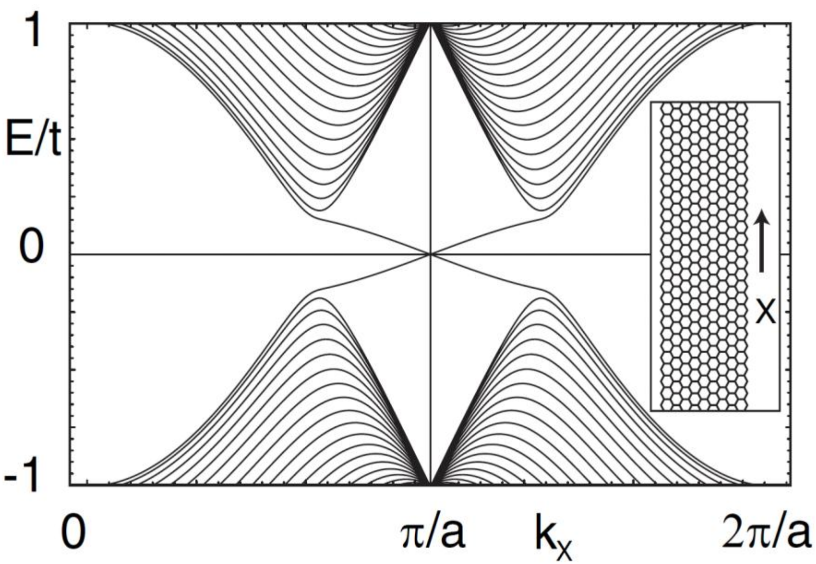

topologically nontrivial

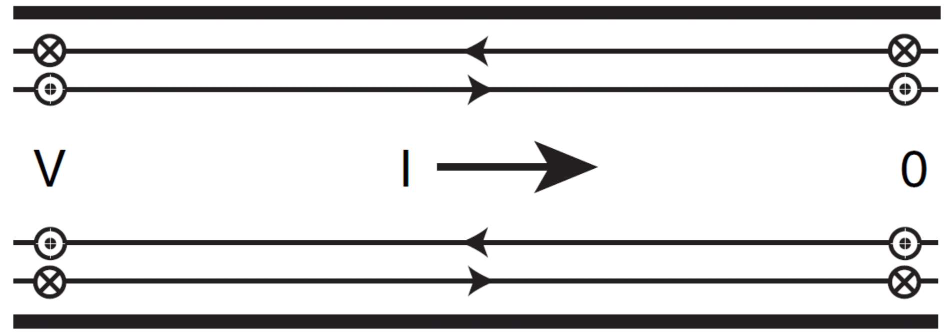

not a practical toplogical insulator (TI) because of weak intrinsic SO coupling

To engineer the TI phase in graphene Theoretical studies have shown that graphene bilayer and trilayer → TI phase under large Rashba interaction and a bias used to open a band-gap

C. Weeks *et al.*, PRX 1, 021001 (2011).

H. Jiang *et al*, PRL 109, 116803 (2012).

Z. Qiao *et al.*, PRL 107, 256801 (2011).

X. Li et al., PRB 85, 201404(R) (2012).

1. Background: HgTe/CdTe quantum wells

The first confirmation of TI theoretically and experimentally

B. A. Bernevig, T. L. Hughes, and S.-C. Zhang, Science 314, 1757 (2006);

M. Konig *et al.*, Science 318, 766 (2007).

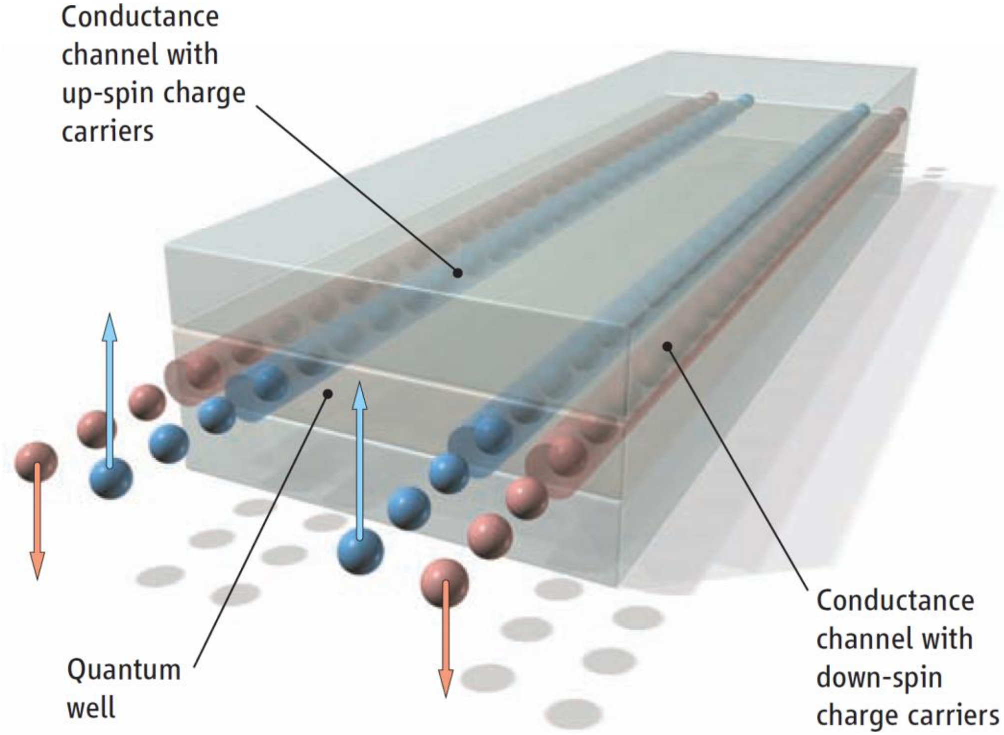

A variant material CdTe/Hg CdTe/CdTe quantum well is possible for transition between a normal insulator (NI) and a topological insulator by an electric field

J. Li and K. Chang, APL 95, 222110 (2009).

further expectation to explore the topological phase transition

1. Background: Boron-nitride mono- and multi-layers

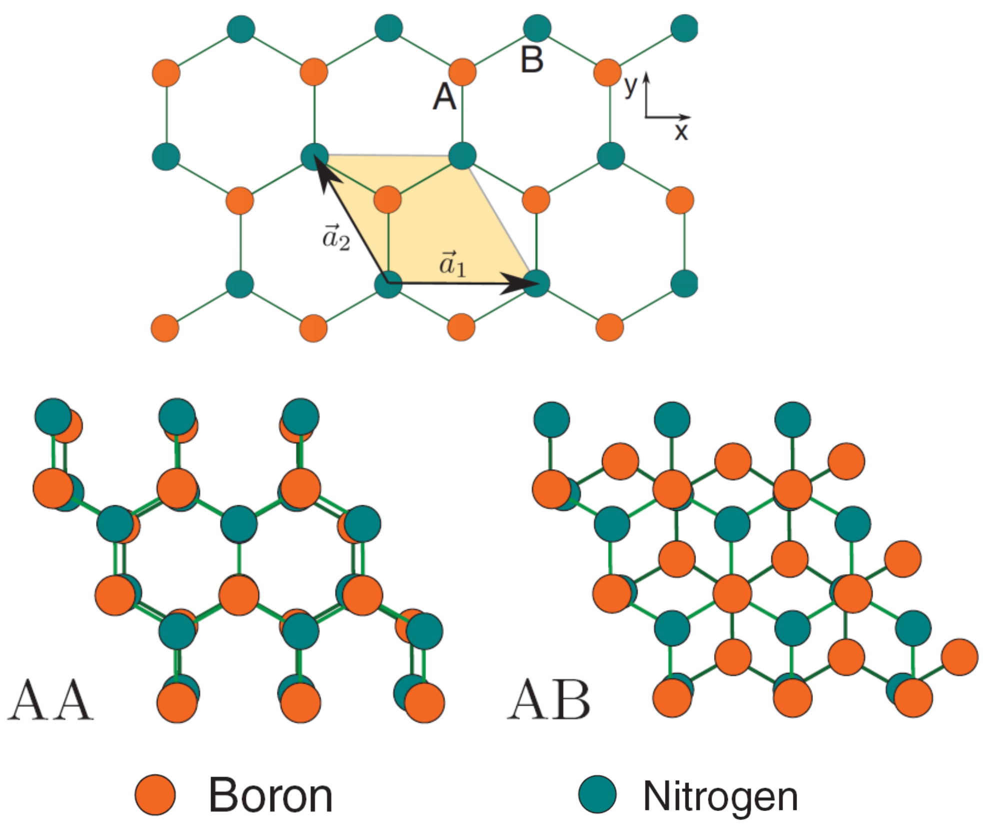

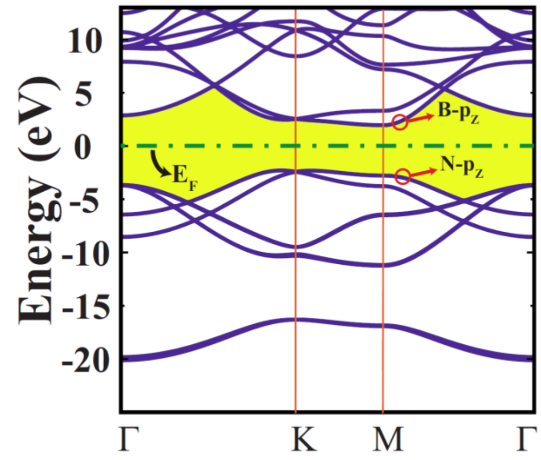

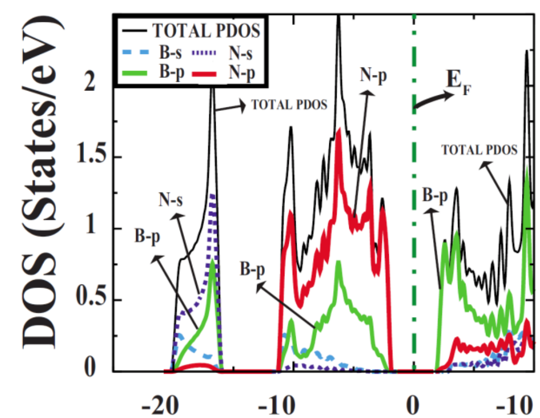

R. M. Ribeiro and N. M. R. Peres, PRB 83, 235312 (2011).

M. Topsakal, E. Aktürk, and S. Ciraci, PRB 79, 115442 (2009).

a hexagonal boron nitride (BN) layer is made out of strong polar covalent bonds and has no reflection symmetry. This leads to large band-gaps, about 4.6 eV for monolayer and 6 eV for single crystal

2. Object and Formulation: Boron-nitride bilayers

We ask Is it possible to realize the TI phase in large-gap BN materials?

We propose a way to significantly reduce their gaps to find TI phase!

Consider two stable stacked boron-nitride bilayers as in figures

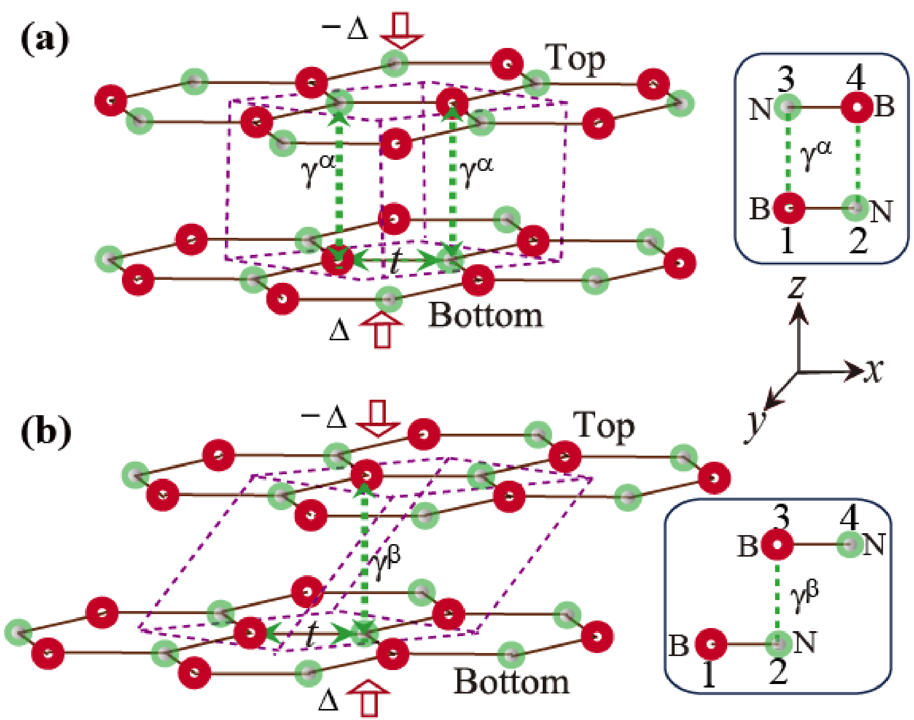

AA-stacked BNBL (α-BNBL)

Δ and –Δ are the electrostatic potential energies created by a gate voltage

AB-stacked BNBL (β-BNBL)

Contrary to a graphene bilayer, the interlayer bias here is used to reduce the charge polarity of two trigonal sublattices in different layers and then to decrease the band-gaps of the two stackings

2. Object and Formulation: Model Hamiltonian

In the tight-binding approximation, Kane-Mele model $+\gamma+\Delta$

$$\mathcal{H} = \mathcal{H}_B + \mathcal{H}_T + \mathcal{H}_{BT} + \mathcal{H}_{TB}$$

$$\mathcal{H}_{B(T)} = \sum_{i\sigma} (\varepsilon_i \pm \Delta) c_{i\sigma}^{\dagger} c_{i\sigma} - t \sum_{\langle ij \rangle \sigma} c_{i\sigma}^{\dagger} c_{j\sigma} + i\lambda_{\mathrm{SO}} \sum_{\langle\langle ij \rangle\rangle \sigma\bar{\sigma}} \nu_{ij} \boldsymbol{S}_{\sigma\bar{\sigma}} \cdot \boldsymbol{z} c_{i\sigma}^{\dagger} c_{j\bar{\sigma}} + i\lambda_{\mathrm{R}} \sum_{\langle ij \rangle \sigma\sigma'} \left(\boldsymbol{S}_{\sigma\sigma'} \times \boldsymbol{d}_{ij} \right) \cdot \boldsymbol{z}\, c_{i\sigma}^{\dagger} c_{j\sigma'};$$

$$\mathcal{H}_{BT} = \gamma \sum_{i\in B, j\in T, \sigma} c_{i\sigma}^{\dagger} c_{j\sigma}; \qquad \mathcal{H}_{TB} = \gamma \sum_{i\in B, j\in T, \sigma} c_{j\sigma}^{\dagger} c_{i\sigma}$$

The energy spectra and physical properties $\longleftarrow$

Green's function and density of states

$$\mathcal{G}_{i\sigma, j\sigma'}(E) = \frac{1}{\Omega_{\mathrm{BZ}}} \int d\boldsymbol{k} \frac{\mathrm{e}^{i\boldsymbol{k}\cdot(\boldsymbol{r}_{i\sigma} - \boldsymbol{r}_{j\sigma'})}}{E + i\eta - \mathcal{H}(\boldsymbol{k})}$$

$$g_\sigma(E) = -\frac{1}{\pi} \sum_{i=1}^{4} \mathrm{Im}\, \mathcal{G}_{i\sigma, i\sigma}(E)$$

2. Object and Formulation: Matrix representation

Hamiltonian in the momentum space, an 8×8 matrix

$$\mathcal{H}(\boldsymbol{k}) = \begin{pmatrix} \mathcal{H}_B(\boldsymbol{k}) & \mathcal{H}_{BT} \\ \mathcal{H}_{TB} & \mathcal{H}_T(\boldsymbol{k}) \end{pmatrix}$$

$$\mathcal{H}_{BT}^{\alpha} = \begin{pmatrix} \gamma^{\alpha}\mathbf{I} & 0 \\ 0 & \gamma^{\alpha}\mathbf{I} \end{pmatrix}, \quad \mathcal{H}_{BT}^{\beta} = \begin{pmatrix} 0 & 0 \\ \gamma^{\beta}\mathbf{I} & 0 \end{pmatrix}$$

$$\mathcal{H}_{B(T)}(\boldsymbol{k}) = \begin{pmatrix} \epsilon_{s1} + d(\boldsymbol{k}) & 0 & f(\boldsymbol{k}) & g_1(\boldsymbol{k}) \\ 0 & \epsilon_{s1} - d(\boldsymbol{k}) & g_2(\boldsymbol{k}) & f(\boldsymbol{k}) \\ f^*(\boldsymbol{k}) & g_2^*(\boldsymbol{k}) & \epsilon_{s2} - d(\boldsymbol{k}) & 0 \\ g_1^*(\boldsymbol{k}) & f^*(\boldsymbol{k}) & 0 & \epsilon_{s2} + d(\boldsymbol{k}) \end{pmatrix}$$

All the matrix elements are determined

$$d(\boldsymbol{k}) = 2\lambda_{\mathrm{SO}}\left[2\sin\left(\sqrt{3}k_y a/2\right)\cos(3k_x a/2) - \sin\left(\sqrt{3}k_y a\right)\right]$$

$$f(\boldsymbol{k}) = -t\mathrm{e}^{ik_x a}\left[1 + 2\mathrm{e}^{-i(3k_x a/2)}\cos\left(\sqrt{3}k_y a/2\right)\right]$$

$$g_1(\boldsymbol{k}) = -\lambda_{\mathrm{R}}\mathrm{e}^{ik_x a}\left[1 - 2\mathrm{e}^{-i(3k_x a/2)}\cos\left(\sqrt{3}k_y a/2 + \pi/3\right)\right]$$

$$g_2(\boldsymbol{k}) = \lambda_{\mathrm{R}}\mathrm{e}^{ik_x a}\left[1 - 2\mathrm{e}^{-i(3k_x a/2)}\cos\left(\sqrt{3}k_y a/2 - \pi/3\right)\right]$$

3. Main Results: (i) Bulk electronic structures

Dispersion relations and the densities of states (DOS) of (a) α-BNBL and (b) β-BNBL

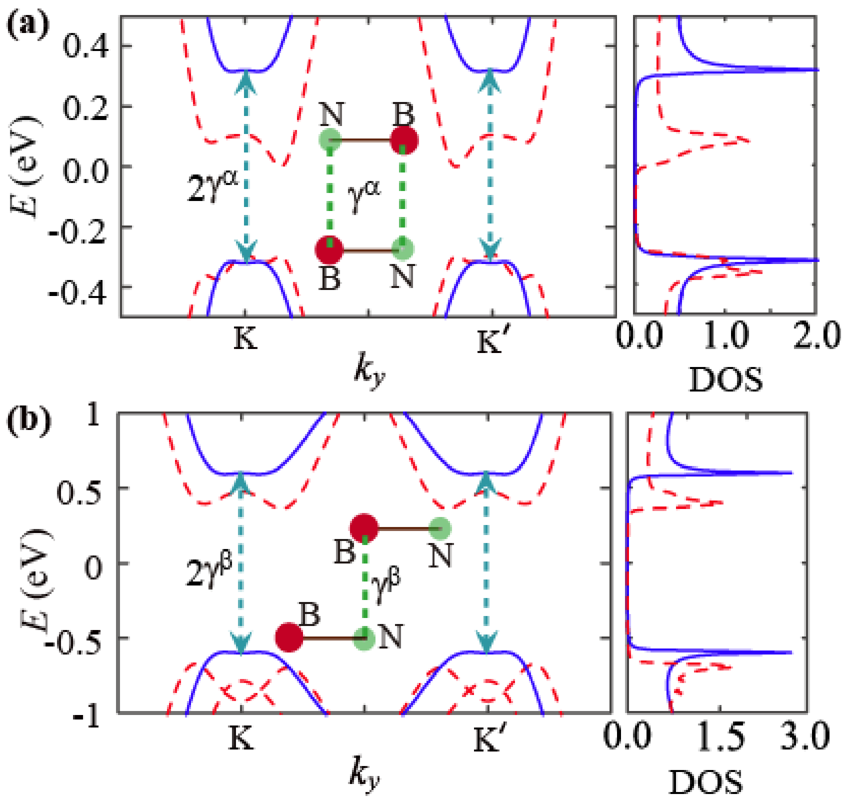

$$E^{\alpha} = \pm\sqrt{\Delta^2 + \left(\varepsilon_0^{\alpha}\right)^2 + (\gamma^{\alpha})^2 + |f(\boldsymbol{k})|^2 \pm 2\sqrt{h^{\alpha}(\boldsymbol{k})}},$$

$$E^{\beta} = \pm\sqrt{\Delta^2 + \left(\varepsilon_0^{\beta}\right)^2 + \frac{1}{2}(\gamma^{\beta})^2 + |f(\boldsymbol{k})|^2 \pm \sqrt{h^{\beta}(\boldsymbol{k})}}$$

The influence of the SO couplings

Solid lines Dashed lines

$\lambda_{\mathrm{SO}} = \lambda_{\mathrm{R}} = 0$ $\lambda_{\mathrm{SO}} = 0.05t^{\alpha(\beta)},\ \lambda_{\mathrm{R}} = 0.2t^{\alpha(\beta)}$

The band-gaps are greatly reduced by the gate voltage, due to the decrease of the charge polarity. For $\Delta = \varepsilon_0^{\alpha(\beta)}$

$E_{\mathrm{g}}^{\alpha} \cong 2\gamma^{\alpha} = 0.64\,\mathrm{eV}$ $E_{\mathrm{g}}^{\beta} \cong 2\gamma^{\beta} = 1.2\,\mathrm{eV}$

$\ll$ 4.6 eV in natural BN layers

$$h^{\alpha}(\boldsymbol{k}) = \Delta^2\left[\left(\varepsilon_0^{\alpha}\right)^2 + |f(\boldsymbol{k})|^2\right] + |\gamma^{\alpha} f(\boldsymbol{k})|^2$$

$$h^{\beta}(\boldsymbol{k}) = 4\Delta^2\left[(\varepsilon_0^{\beta})^2 + |f(\boldsymbol{k})|^2\right] - 2\Delta\varepsilon_0^{\beta}\left(\gamma^{\beta}\right)^2 + |\gamma^{\beta} f(\boldsymbol{k})|^2 + \frac{1}{4}\left(\gamma^{\beta}\right)^4$$

3. Main Results: (ii) Edge states and Z_2 topological index

Particular concern is to find the topological edge states for the confined boron-nitride bilayer nanoribbons (NR) in Figure

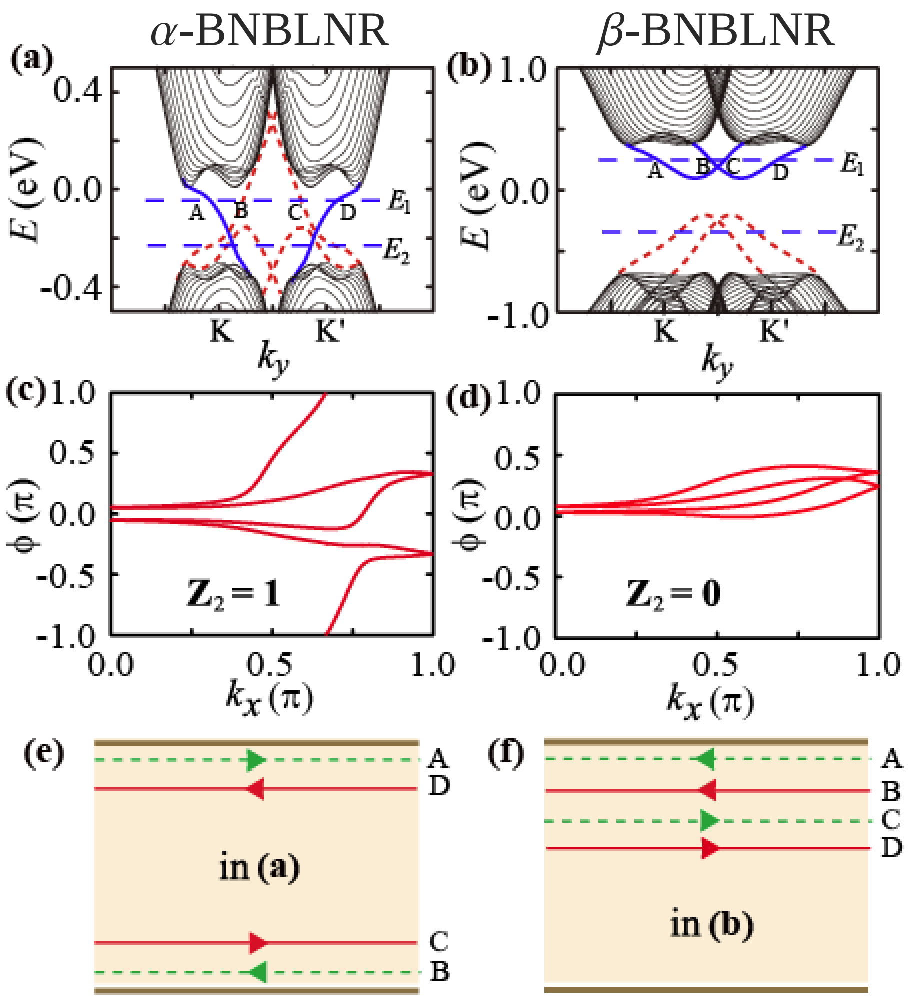

(a), (b) show the band structures of the α- and β-BNBLNRs with

$$\lambda_{SO} = 0.05t^{\alpha(\beta)},\ \lambda_R = 0.2t^{\alpha(\beta)}$$

There are edge states within the bulk gaps, their dispersion curves

(c), (d) illustrate the evolution lines of the Wannier function centers used

$$\Rightarrow \quad Z_2 = \sum_{n=1}^{4} T_n \bmod 2 = \begin{cases} 1, & \text{T I} \\ 0, & \text{not T I} \end{cases}$$

(e), (f) distribute the four edge states A, B, C, D in (a), (b). α-BNBLNR has the feature of TI, β-BNBLNR has not

3. Main Results: (iii) Phase diagram and edge transport

The condition of forming the topological edge states in the α-BNBLNR. For a nonzero λ_{SO}, obtain analytically

Two phase boudaries: $\lambda_R \sim \Delta$

$$\lambda_R = \frac{\sqrt{2}}{3}\sqrt{54\lambda_{SO}^2 - 6\lambda_{SO}\sqrt{3\eta_1} + \Delta\chi + (\gamma^\alpha)^2 \pm \sqrt{\zeta}}$$

$$\zeta = 12\lambda_{SO}\left(9\lambda_{SO} - \sqrt{3\eta_1}\right)\eta_2 + \Delta^2\chi^2 + (\gamma^\alpha)^2\left[(\gamma^\alpha)^2 + 2\Delta\chi\right]$$

$$\chi \equiv \Delta - \varepsilon_0^\alpha,\ \eta_1 \equiv (\gamma^\alpha)^2 + \chi^2,\ \eta_2 \equiv (\gamma^\alpha)^2 + \Delta^2$$

Figure (a) The phase diagram divided into three parts: NI, TI, NI; P_1, P_2, P_3; as the bias increases, the reentrant phase behavior takes place;
right insets show the energy bands of three points A, B, C; for $\Delta>\Delta_c$

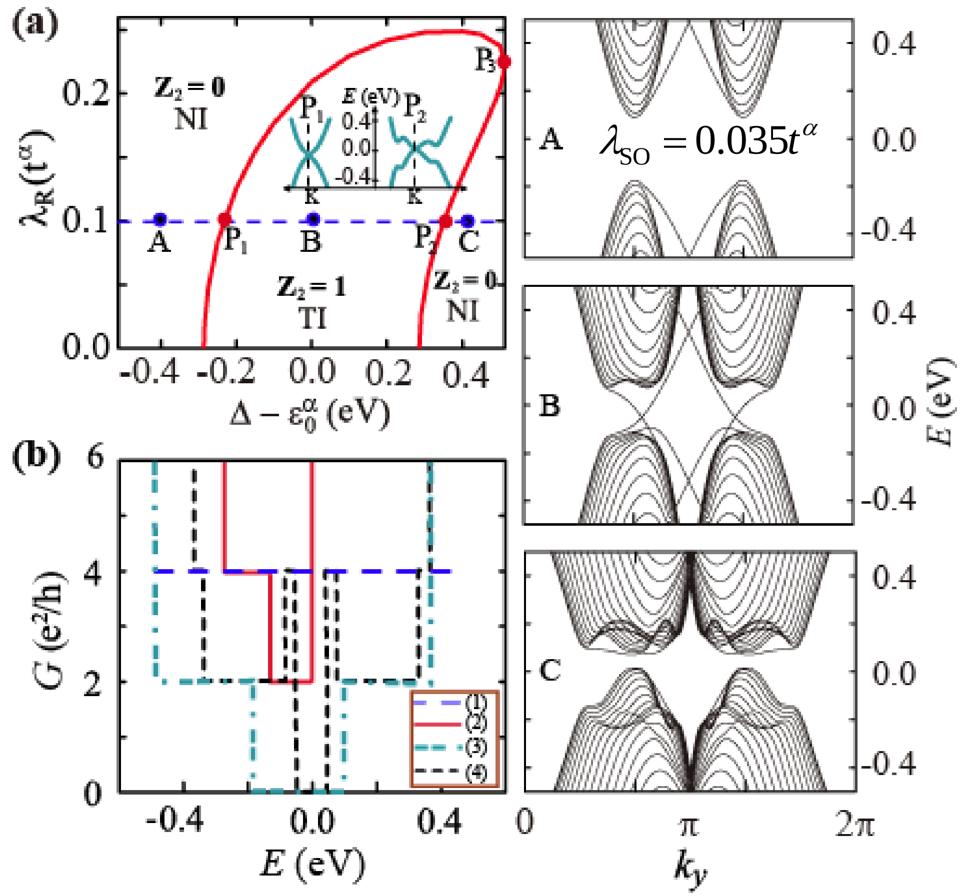

Figure (b) shows the quantized edge conductance ~ energy in the different constructions and parameters.

$$G(E) = e^2/h\ \mathrm{Tr}[\mathcal{G}^r(E)\Gamma_L(E)\mathcal{G}^a(E)\Gamma_R(E)]$$

4. Summary: Some conclusions

For large-gap boron nitride, bias voltage can drive it to

1) A strong TI phase has been found in the AA-stacked BNBL, while the AB-stacked BNBL is impossible to become a TI.
2) For the AA-stacked BNBL, a reentrant behavior from an NI phase to a TI phase and then to an NI phase has been confirmed, and the two phase boundaries have been analytically given.
3) For the AB-stacked BNBL, four degenerate low-energy edge states are localized at a single edge

四. *Rashba* 自旋轨道作用下碳单层和双层中反转的 *Berry* 相位和 *Andreev* 反射

X. Zhai and G. Jin, PRB **89**, 085430 (2014).

1. Background: Chirality and Berry phase

GML:

$$\mathcal{H}_{\mathbf{K}} = \hbar v_F \boldsymbol{k}.\hat{\boldsymbol{\sigma}} = \hbar v_F \begin{pmatrix} 0 & k_x - ik_y \\ k_x + ik_y & 0 \end{pmatrix}$$

GBL:

$$\mathcal{H}_{\mathbf{K}} = -\frac{\hbar^2}{2m^*} \begin{pmatrix} 0 & (k_x - ik_y)^2 \\ (k_x + ik_y)^2 & 0 \end{pmatrix}$$

$$E(\boldsymbol{k}) = \pm \hbar v_F |\boldsymbol{k}|$$

$$E(\boldsymbol{k}) = \pm \frac{(\hbar \boldsymbol{k})^2}{2m^*}$$

$$\psi_{\pm,\mathbf{K}}(\boldsymbol{k}) = \frac{1}{\sqrt{2}} \begin{pmatrix} 1 \\ \pm e^{i\theta_{\boldsymbol{k}}} \end{pmatrix}$$

$$\hat{C} \equiv \frac{\boldsymbol{k} \cdot \hat{\boldsymbol{\sigma}}}{k}$$

$$\psi_{\pm,\mathbf{K}}(\boldsymbol{k}) = \frac{1}{\sqrt{2}} \begin{pmatrix} 1 \\ \mp e^{2i\theta_{\boldsymbol{k}}} \end{pmatrix}$$

Berry phase-π

$$\Phi_B = i \oint_C dk \left\langle \psi(k) \left| \frac{\partial}{\partial k} \right| \psi(k) \right\rangle$$

Berry phase-2π

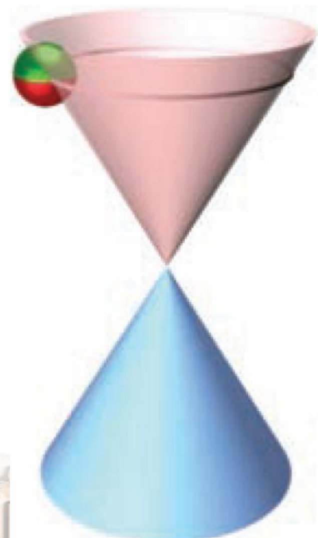

Berry phase in graphene from quantum Hall effect:

Y. Zhang et al., Nature 438, 201 (2005).

K. S. Novoselov et al., Nat. Phys. 2, 177 (2006).

Berry phase in graphene from weak antilocalization:

X. Wu et al., PRL 98, 136801 (2007).

Berry phase in graphene from photoemission:

Y. Liu et al., PRL 107, 166803 (2011).

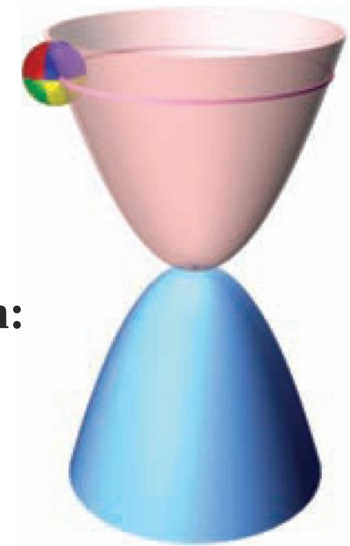

1. Background: Andreev reflection

GML: C. W. J. Beenakker, PRL 97, 067007 (2006). “Specular Andreev reflection in graphene”

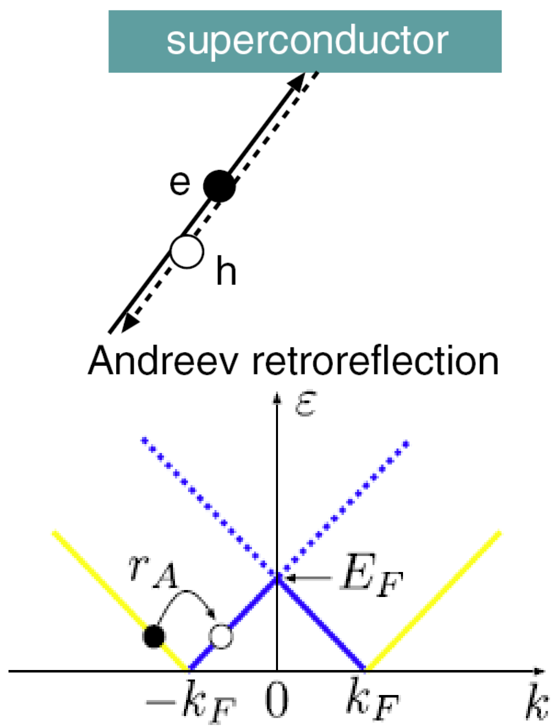

Andreev retroreflection

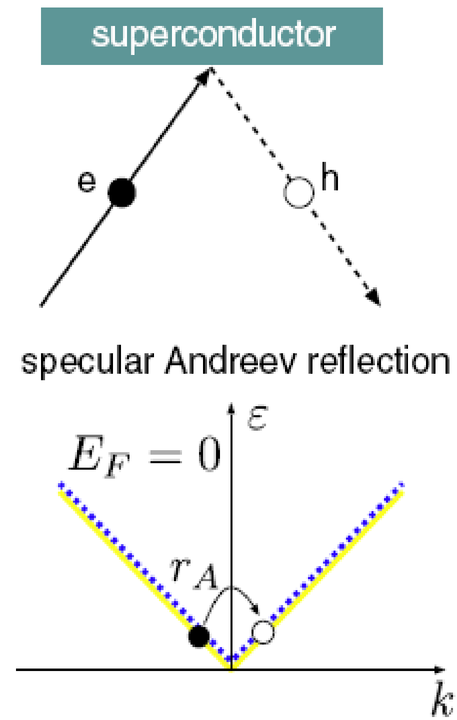

specular Andreev reflection

入射导带电子：若反射空穴来自电子导带，则发生回射；若反射空穴来自电子价带，则发生镜面反射 。

GBL: T. Ludwig, PRB 75, 195322 (2007). “Andreev reflection in bilayer graphene”

1. Background: Theoretical treatment

Bogoliubov-de Gennes (BdG) 方程

$$\begin{pmatrix} \mathcal{H}_{\mathbf{K}(\mathbf{K}')} - E_{\mathrm{F}} & \Delta_0 e^{i\phi}\Theta(x) \\ \Delta_0 e^{-i\phi}\Theta(x) & E_{\mathrm{F}} - \mathcal{H}_{\mathbf{K}(\mathbf{K}')} \end{pmatrix} \begin{pmatrix} u \\ v \end{pmatrix} = \varepsilon \begin{pmatrix} u \\ v \end{pmatrix}$$

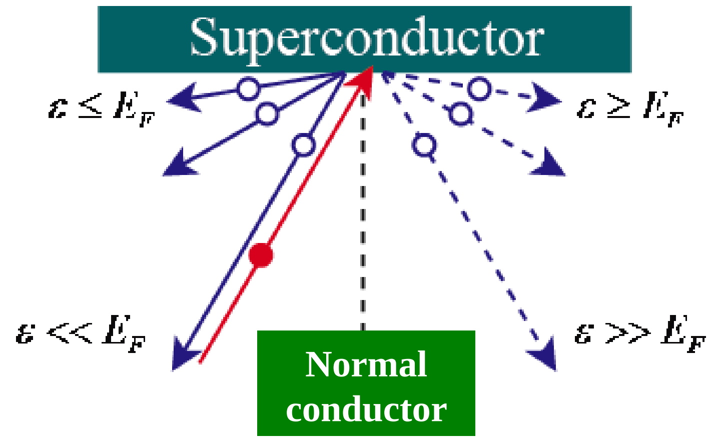

对角化得到能谱

$$\varepsilon = \left|E_{\mathrm{F}} \pm \hbar v_{\mathrm{F}}\sqrt{k_x^2 + k_y^2}\right|$$

$$\frac{G}{G_0} = \int_0^{\pi/2} d\theta \cos\theta[1 - R(eV,\theta) + R_{\mathrm{A}}(eV,\theta)]$$

(both no Rashiba coupling)

GML:

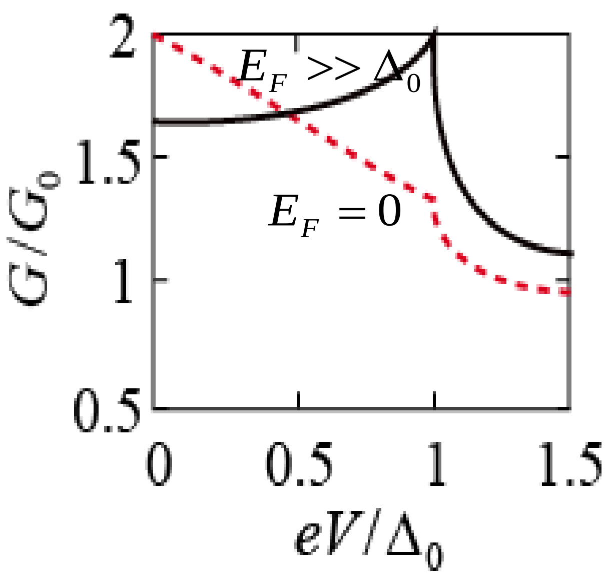

GBL:

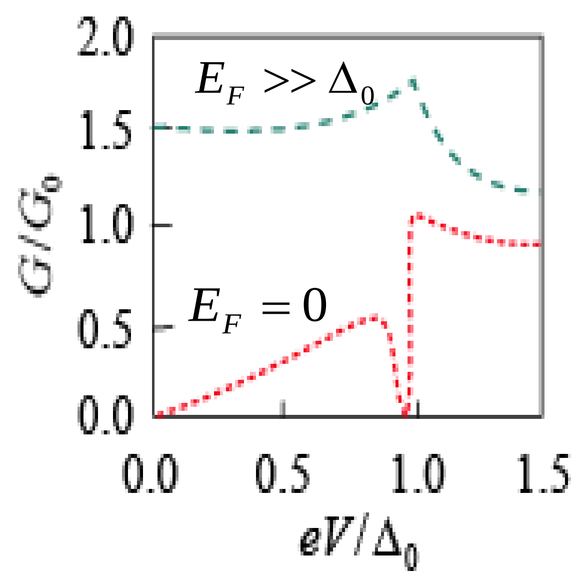

2. Object and Formulation: 碳单层和双层中的Rashba 作用

碳单层实验：D. Marchenko et. al., Nature Commun. 3, 1232 (2012).

Au 插层 5d 电子邻近诱导 Rashba 作用

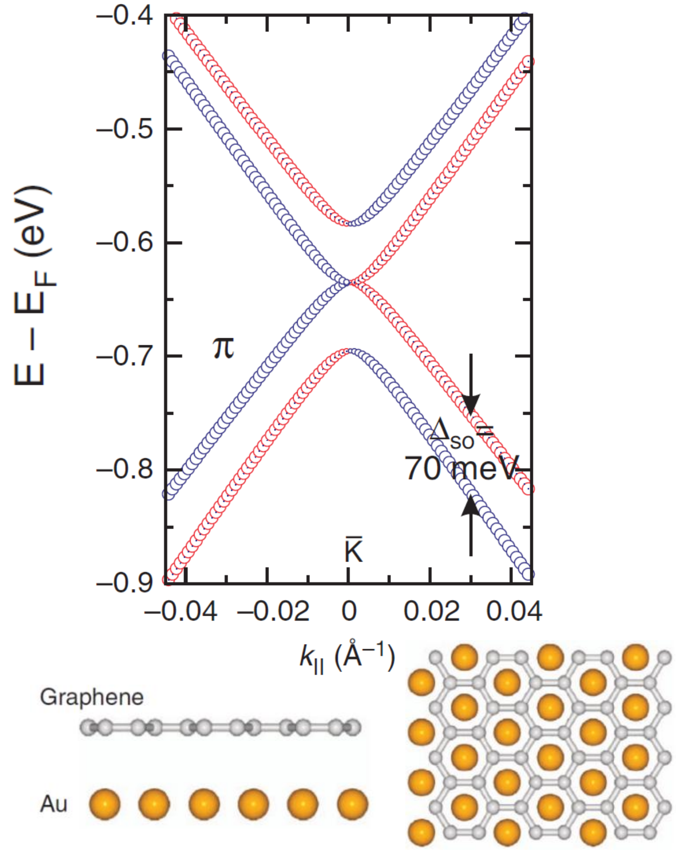

$$H = t\sum_{\langle ij\rangle} c_i^\dagger c_j + i\lambda_R \sum_{\langle ij\rangle} c_i^\dagger (\mathbf{s}\times\hat{\mathbf{d}}_{ij})_z c_j$$

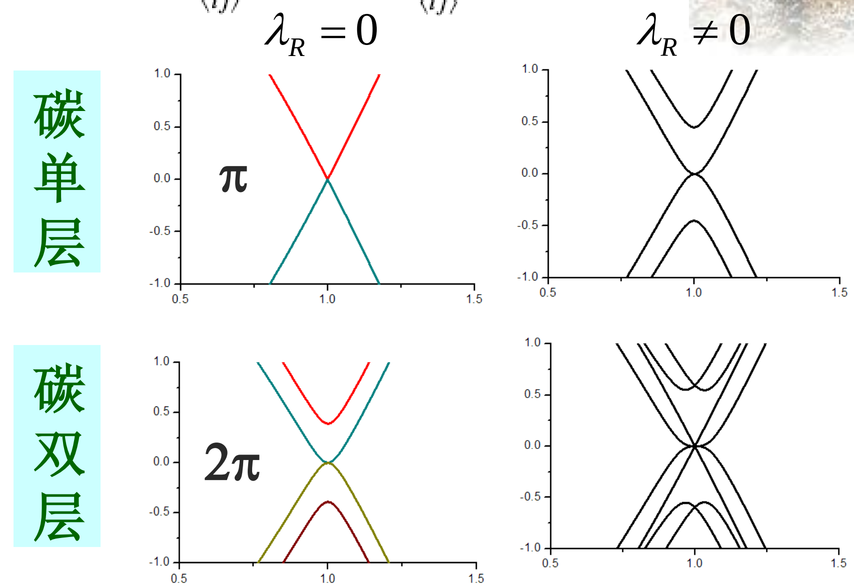

Berry 相位表征的能带拓扑发生改变

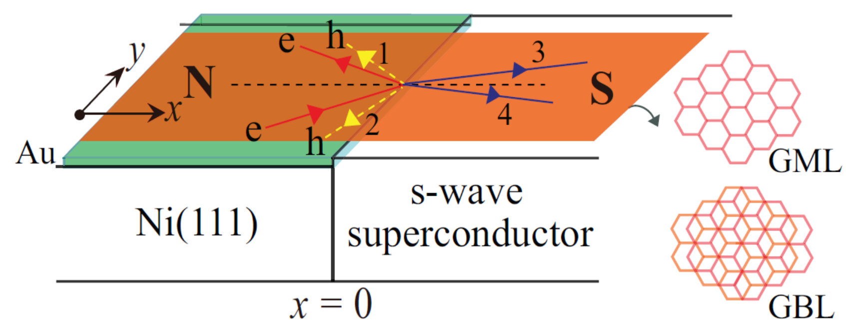

关于 Rashba 相互作用的理论工作：E. I. Rashba, Phy. Rev. B, 79, 161409(R) (2009).
M.-H. Liu, et al., Phy. Rev. B, 85, 085406 (2012).

吸附 In 原子未增强 自旋轨道耦合：Z. Jia et al., Phys. Rev. B 91, 085411 (2015).

2. Object and Formulation: 能谱、波函数和 Berry 相位

Matrix representation with Rashiba interaction

碳单层

$$\mathcal{H}_\xi = \hbar v_{\rm F}(\sigma_x k_x + \xi\sigma_y k_y)\otimes s_0 + \frac{\lambda_{\rm R}}{2}(\sigma_x\otimes s_y - \xi\sigma_y\otimes s_x)$$

$$E_{\mu\nu}(k) = \frac{\mu\nu}{2}\left(\sqrt{\lambda_{\rm R}^2 + 4(\hbar v_{\rm F}k)^2} - \nu\lambda_{\rm R}\right)$$

$$\psi^{\rm K}_{\mu+} = c_0(i\mu\varrho e^{-i\theta}, \mu\varrho', i\varrho', \varrho e^{i\theta})^{\rm T}$$

$$\psi^{\rm K}_{\mu-} = c_0(i\mu\varrho' e^{-i\theta}, -\mu\varrho, -i\varrho, \varrho' e^{i\theta})^{\rm T}$$

$$\psi^{\rm K'}_{\mu+} = c_0(\mu\varrho', -i\mu\varrho e^{i\theta}, \varrho e^{-i\theta}, -i\varrho')^{\rm T}$$

$$\psi^{\rm K'}_{\mu-} = c_0(-\mu\varrho, -i\mu\varrho' e^{i\theta}, \varrho' e^{-i\theta}, i\varrho)^{\rm T}$$

$\varrho = \cos(\vartheta/2)$， $\varrho' = \sin(\vartheta/2)$

$$\Phi_{\rm B} = i\int_0^{2\pi} d\theta \left\langle \psi^\xi_{\mu\nu}\left|\frac{\partial}{\partial\theta}\right|\psi^\xi_{\mu\nu}\right\rangle = 0$$

可以证明，使用另外的一个规范，用 $\psi^\xi_{\mu\nu}$ 乘以$e^{-i\theta}$；$\Phi_{\rm B}$ 变成 2π。因此，规范只是改变了赝自旋的绕数

$\boxed{\text{Berry 相位从 } \pi\ (\lambda_{\rm R}=0) \text{ 变为 } 2\pi\ (\lambda_{\rm R}\neq 0)}$

碳双层

$$\mathcal{H}_\xi = H^0_\xi + H^{\rm R}_\xi = -\frac{(\hbar v_F k)^2}{\gamma}\begin{pmatrix} 0 & e^{-2i\xi\theta} \\ e^{2i\xi\theta} & 0 \end{pmatrix}\otimes s_0$$

$$-\frac{\hbar v_{\rm F}\lambda_{\rm R}}{\gamma}[\sigma_x\otimes(k_x s_y + k_y s_x) - \xi\sigma_y\otimes(k_x s_x - k_y s_y)]$$

$$E_{\mu\nu}(k) = \frac{\mu\hbar v_{\rm F}k}{\gamma}\left(\sqrt{\lambda_{\rm R}^2 + (\hbar v_F k)^2} - \nu\lambda_{\rm R}\right)$$

$$\psi^{\rm K}_{\mu+} = c_0(-i\mu\varrho e^{-2i\theta}, -\mu\varrho' e^{-i\theta}, i\varrho', \varrho e^{i\theta})^{\rm T}$$

$$\psi^{\rm K}_{\mu-} = c_0(i\mu\varrho' e^{-2i\theta}, -\mu\varrho e^{-i\theta}, -i\varrho, \varrho' e^{i\theta})^{\rm T}$$

$$\psi^{\rm K'}_{\mu+} = c_0(-\mu\varrho' e^{i\theta}, i\mu\varrho e^{2i\theta}, \varrho e^{-i\theta}, -i\varrho')^{\rm T}$$

$$\psi^{\rm K'}_{\mu-} = c_0(-\mu\varrho e^{i\theta}, -i\mu\varrho' e^{2i\theta}, \varrho' e^{-i\theta}, i\varrho)^{\rm T}$$

$\varrho = \cos(\vartheta/2)$, $\varrho' = \sin(\vartheta/2)$， $\vartheta = \arctan(\hbar v_F k/\lambda_{\rm R})$

$$\Phi_{\rm B} = i\int_0^{2\pi} d\theta \left\langle \psi^\xi_{\mu\nu}\left|\frac{\partial}{\partial\theta}\right|\psi^\xi_{\mu\nu}\right\rangle = \begin{cases} \pi, & \text{for } \psi^{\rm K}_{\mu\nu} \\ -\pi, & \text{for } \psi^{\rm K'}_{\mu\nu} \end{cases}$$

$\boxed{\text{Berry 相位从 } 2\pi\ (\text{对于 } \lambda_{\rm R}=0) \text{ 变为 } \pi\ (\text{对于 } \lambda_{\rm R}\neq 0)}$

3. Main Results: Rashba 作用反转 Berry 相位后的能谱

未掺杂时，E_F=0，在 K 或 K′ 谷附近

碳单层　　　　碳双层

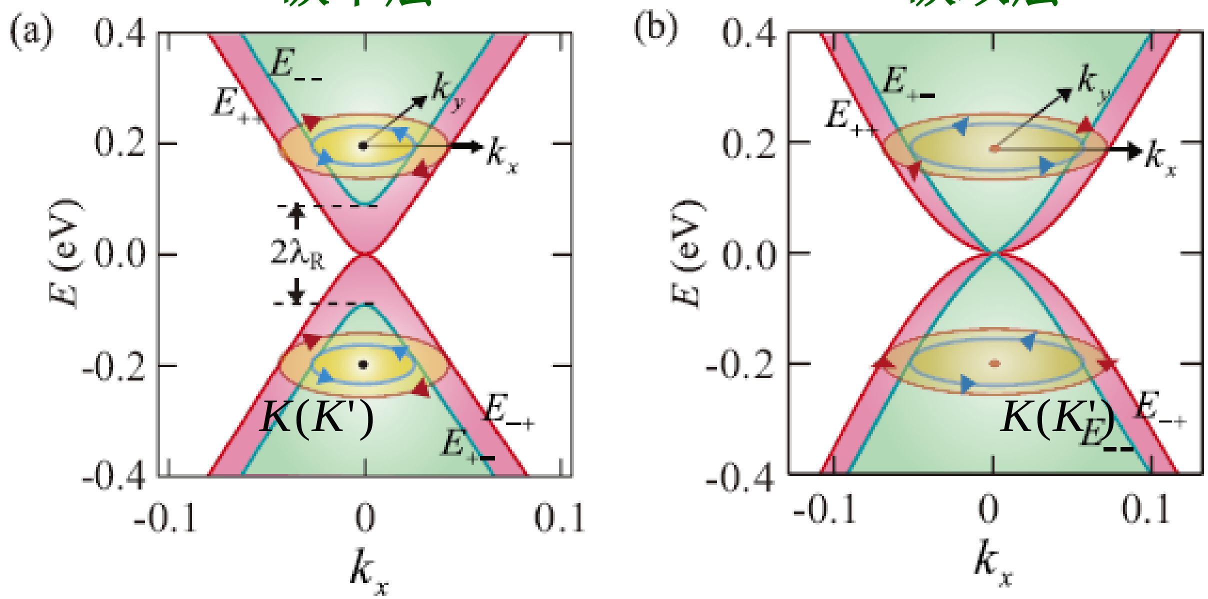

真实自旋算符 $\sigma_0 \otimes s$ 和赝自旋算符 $\sigma \otimes s_0$ 的平均值

$$\langle \sigma_0 \otimes s \rangle_{\mu\nu} = (\boldsymbol{e}_k \times \boldsymbol{z})\, \nu \sin\vartheta$$

$$\langle \sigma \otimes s_0 \rangle_{\mu\nu} = \boldsymbol{e}_k\, \mu\nu \sin\vartheta$$

$$\begin{aligned}\langle \sigma_0 \otimes s \rangle_{\mu\nu} &= (\boldsymbol{e}_k \times \boldsymbol{z})\, \nu \sin\vartheta \\ \langle \sigma \otimes s_0 \rangle_{\mu\nu} &= -\mu \sin\vartheta[\boldsymbol{x}\cos(2\theta) \\ &\quad + \xi \boldsymbol{y} \sin(2\theta)]\end{aligned}$$

下面考虑：NS 结上的电子-空穴转换！

3. Main Results: Analysing incidence and reflection

BdG equation

$$\begin{pmatrix} \mathcal{H}_\xi(x) - E_\mathrm{F} & \Delta\Theta(x) \\ \Delta^*\Theta(x) & E_\mathrm{F} - \mathcal{H}_\xi(x) \end{pmatrix} \begin{pmatrix} u \\ v \end{pmatrix} = \varepsilon \begin{pmatrix} u \\ v \end{pmatrix}$$

$$\mathcal{H}_\xi(x) = \mathcal{H}_\xi^0 + \mathcal{H}_\xi^\mathrm{R}\Theta(-x) - U_0\Theta(x)$$

Excitation spectrum

$$\varepsilon_{\mu\nu} = \frac{1}{2}\left| \sqrt{\lambda_\mathrm{R}^2 + 4(\hbar v_F k)^2} - \nu\lambda_\mathrm{R} - 2\mu\nu E_\mathrm{F} \right| \quad \text{(N)}$$

$$\varepsilon_{\mu\nu} = \sqrt{\Delta_0^2 + (E_\mathrm{F}' + \mu\nu\cdot\hbar v_\mathrm{F} k)^2} \quad \text{(S)}$$

Taking an example: Equal energy surface of GML

I: $E_\mathrm{F}=0\ll\Delta_0$

II: $E_\mathrm{F}\gg\Delta_0$

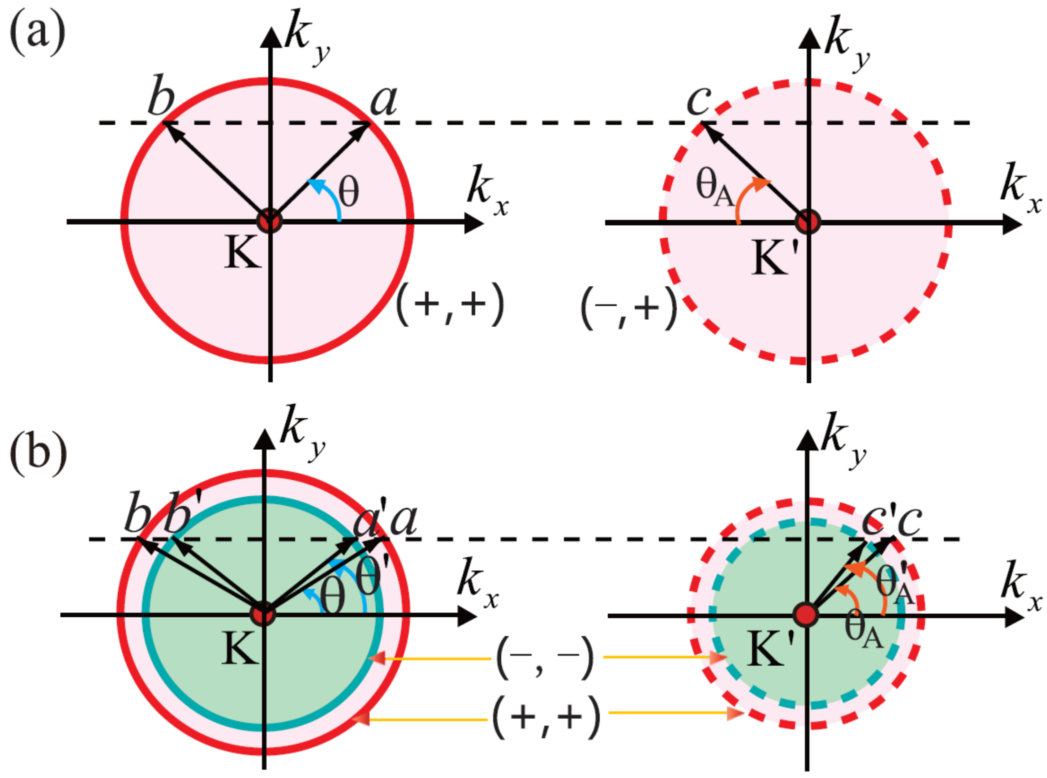

3. Main Results: Excitation spectra at normal incidence

I: $E_F=0$ II: $E_F \gg \Delta_0$

GML

GBL

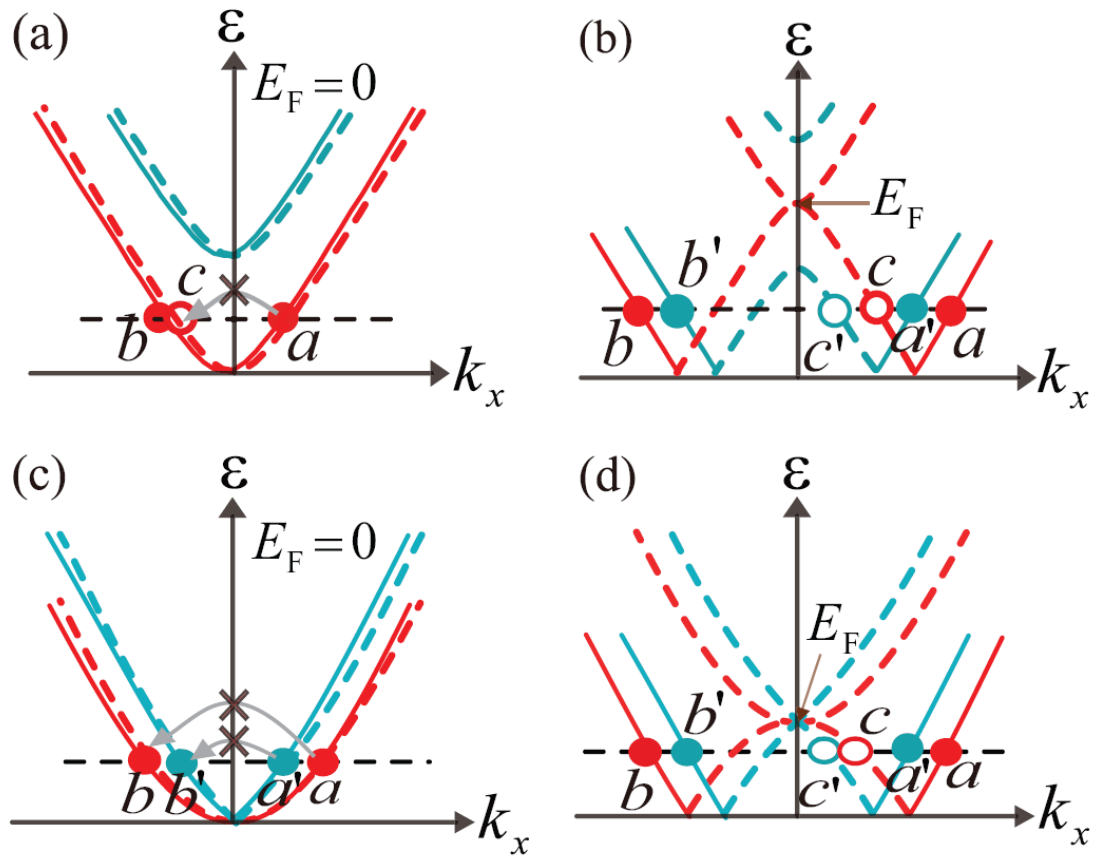

$$\varepsilon_{\mu\nu} = \left| \frac{\hbar v_F k}{\gamma} \left(\sqrt{\lambda_R^2 + (\hbar v_F k)^2} - \nu \lambda_R \right) - \mu E_F \right| \quad \varepsilon_{\mu\nu} = \sqrt{\Delta_0^2 + \left[E_F' + \mu (\hbar v_F k)^2 / \gamma \right]^2}$$

3. Main Results: Interface scattering at an NS junction

The problem can be studied by using the BTK formalism, i.e., solving the BdG equations in both sides of the junction subject to the boundary conditions at the interface

BTK formula: multiband scattering

$$|a\rangle + (r_1|b\rangle + r_2|b'\rangle) + (r_{A_1}|c\rangle + r_{A_2}|c'\rangle) = (t_{1+}|f_+\rangle + t_{2+}|g_+\rangle) + (t_{1-}|f_-\rangle + t_{2-}|g_-\rangle),$$

$$|a'\rangle + (r'_1|b\rangle + r'_2|b'\rangle) + (r'_{A_1}|c\rangle + r'_{A_2}|c'\rangle) = (t'_{1+}|f_+\rangle + t'_{2+}|g_+\rangle) + (t'_{1-}|f_-\rangle + t'_{2-}|g_-\rangle).$$

$$\frac{G}{G_0} = \frac{1}{\mathcal{N}_0}\int_0^{\pi/2} d\theta\cos\theta\Big[\mathcal{N}_1\Big(1-|r_1|^2 - P_{b'}|r_2|^2 + P_c|r_{A_1}|^2 + P_{c'}|r_{A_2}|^2\Big) + \mathcal{N}_2\Big(1-|r'_1|^2 - P_{b'}|r'_2|^2 + P_c|r'_{A_1}|^2 + P_{c'}|r'_{A_2}|^2\Big)\Big]$$

$$G_0 \equiv \partial I_0/\partial V = (2e^2/h)\mathcal{N}_0$$

G. E. Blonder, M. Tinkham, and T. M. Klapwijk, PRB 25, 4515 (1982).

3. Main Results: 亚带隙微分电导可测量信号

碳单层

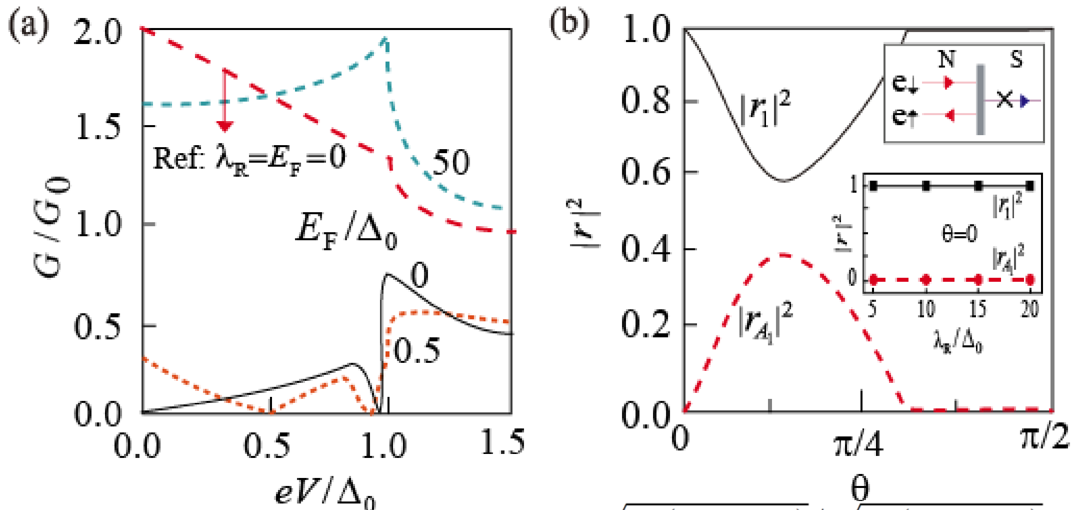

$$\theta_c = \arcsin\sqrt{\varepsilon_-(\varepsilon_- + \lambda_R)}/\sqrt{\varepsilon_+(\varepsilon_+ + \lambda_R)} \simeq 0.278\pi$$

碳双层

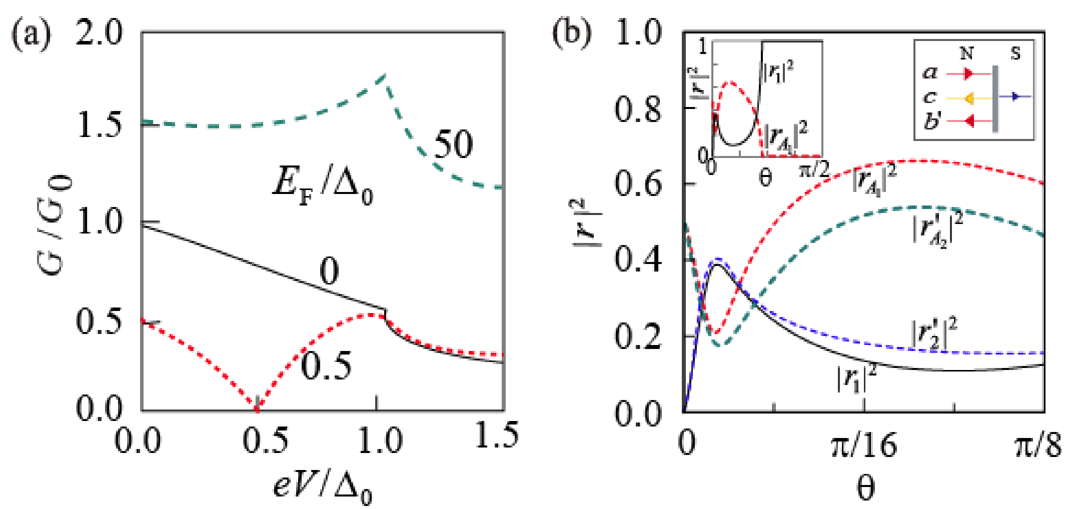

处理方法：**Blonder-Tinkham-Klapwijk** 微分电导计算的理论

4. Summary: Some conclusions

对照无 Rashba 作用的碳单层和双层，新的结果是

1. Rashba 作用可以驱动碳单层、碳双层系统产生 Berry 相位的反转：碳单层从 π 变为 2π，碳双层由 2π 变为 π；
2. 反转 Berry 相位引起正常导体-超导体界面电子-空穴转换的改变，从而导致异常的 Andreev 反射；
3. 反转 Berry 相可以通过正常导体-超导体结的微分电导信号的显著增强和减弱进行测量；
4. 可以考虑其它可能的实验测量

五. 外延和辐照共存时

碳单层的 *Floquet*

拓扑相和热磁效应

X. Zhai and G. Jin, PRB **89**, 235416 (2014).

X. Zhou, Y. Xu, and G. Jin, in preparation.

1. Background：

SiC 衬底上碳单层能带及 Berry 曲率

吴孝松, 物理, **38**,409 (2009).
碳化硅表面的外延 gaphene

低能体能带: 几个 meV 至上百个 meV 的带隙

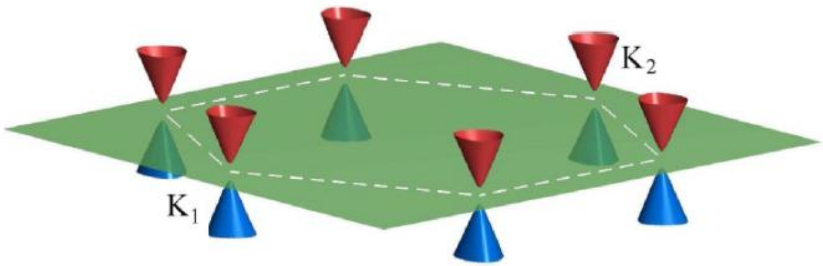

价带的Berry 曲率

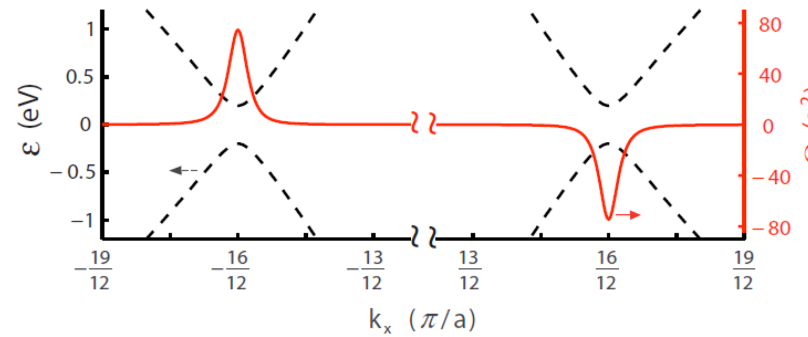

$$\mathcal{H}_{0,\xi}(\boldsymbol{k}) = \hbar v_{\mathrm{F}}(\sigma_x k_x + \xi\sigma_y k_y)$$

$$\mathcal{H}_{\mathrm{s},\xi}(\boldsymbol{k}) = \mathcal{H}_{0,\xi}(\boldsymbol{k}) + \Delta\sigma_z$$

$$\boldsymbol{v}_n(\boldsymbol{k}) = \frac{\partial\varepsilon_n(\boldsymbol{k})}{\hbar\partial\boldsymbol{k}} - \frac{e}{\hbar}\boldsymbol{E}\times\boldsymbol{\Omega}_n(\boldsymbol{k})$$

$$\boldsymbol{\Omega}_n(\boldsymbol{k}) = i\langle\nabla_{\boldsymbol{k}}u_n(\boldsymbol{k})| \times |\nabla_{\boldsymbol{k}}u_n(\boldsymbol{k})\rangle$$

$$\Omega_-(\boldsymbol{k}) = -\xi\frac{(\hbar v_{\mathrm{F}})^2\Delta}{2[\Delta^2 + (\hbar v_{\mathrm{F}}k)^2]^{3/2}}$$

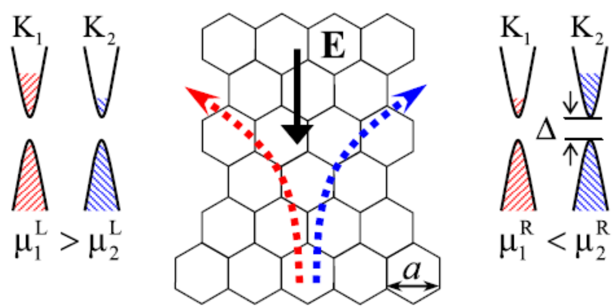

谷 Hall 效应

D. Xiao, W. Yao, and Q. Niu, PRL **99**, 236809 (2007).
D. Xiao, M-C. Chang, and Q. Niu, RMP **82**, 1959 (2010).

1. Background：

圆偏振光诱导的碳单层拓扑相变

$$\mathbf{A}(t) = A[\eta \sin(\omega t)\boldsymbol{e}_x + \cos(\omega t)\boldsymbol{e}_y]$$

$$\mathcal{H}_\xi(\boldsymbol{k}, t) = \hbar v_{\mathrm{F}}\left[\sigma_x\left(k_x + \frac{eA_x(t)}{\hbar}\right) + \xi\sigma_y\left(k_y + \frac{eA_y(t)}{\hbar}\right)\right]$$

$$\mathcal{H}_{\mathrm{F},\xi}(\boldsymbol{k}) \simeq \mathcal{H}_{0,\xi}(\boldsymbol{k}) + \frac{[\mathcal{H}_{-1,\xi}, \mathcal{H}_{+1,\xi}]}{\hbar\omega}$$

$$\mathcal{H}_{m,\xi}(\boldsymbol{k}) = \frac{1}{T}\int_0^T \mathrm{d}t e^{im\omega t}\mathcal{H}_\xi(\boldsymbol{k}, t)$$

$$\mathcal{H}_{\mathrm{F},\xi}(\boldsymbol{k}) = \mathcal{H}_{0,\xi}(\boldsymbol{k}) + \xi F_\eta(\omega)\sigma_z$$

$$= \begin{pmatrix} \xi F_\eta(\omega) & \hbar v_{\mathrm{F}}(k_x - i\xi k_y) \\ \hbar v_{\mathrm{F}}(k_x + i\xi k_y) & -\xi F_\eta(\omega) \end{pmatrix}$$

$$F_\eta(\omega) = \eta(eAv_{\mathrm{F}})^2/\hbar\omega$$

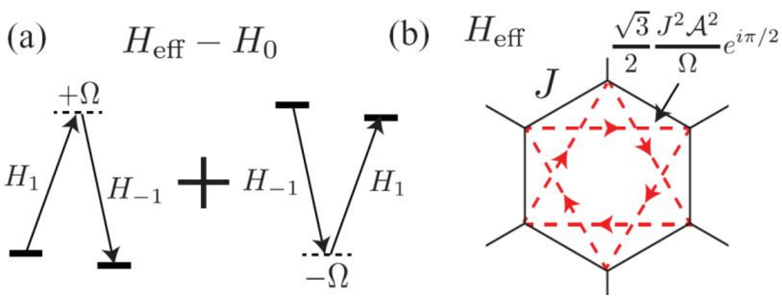

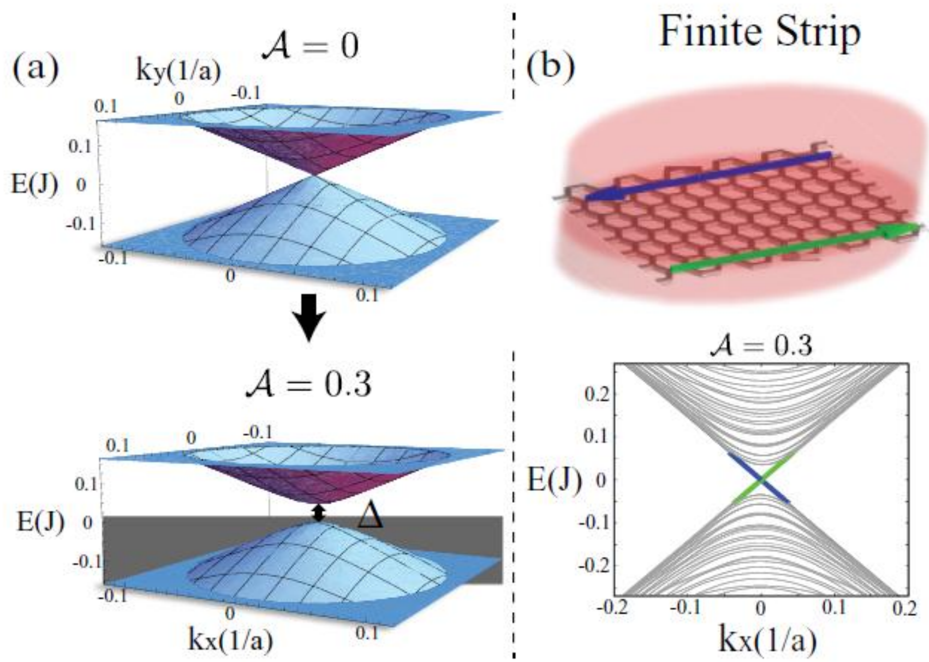

$$E_{\xi,\mathrm{g}} = 2|\xi F_\eta(\omega)| = 2(eAv_{\mathrm{F}})^2/\hbar\omega$$

T. Kitagawa, T. Oka, A. Brataas, L. Fu, and E. Demler, PRB **84**, 235108 (2011).

2. Our Motivation:

考虑衬底和光照共存时的拓扑相变

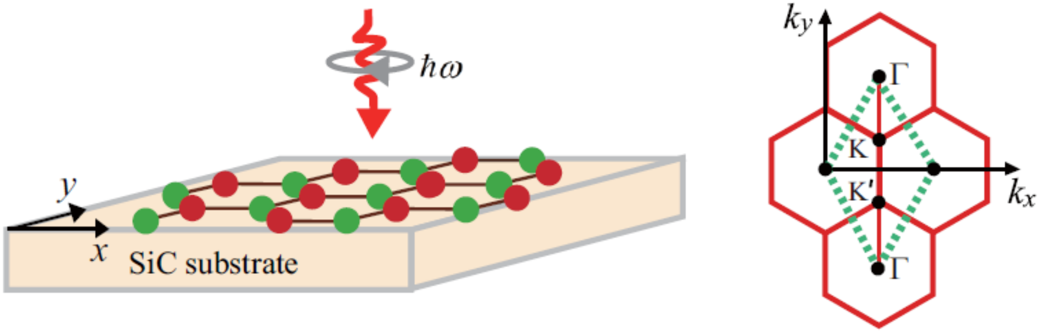

$$\boldsymbol{A}(t) = A_x(t)\boldsymbol{e}_x + A_y(t)\boldsymbol{e}_y = A[\eta \sin(\omega t)\boldsymbol{e}_x + \cos(\omega t)\boldsymbol{e}_y]$$

$$\mathcal{H}_\xi(\boldsymbol{k}, t) = \hbar v_{\mathrm{F}}\left[\sigma_x\left(k_x + \frac{eA_x(t)}{\hbar}\right) + \xi\sigma_y\left(k_y + \frac{eA_y(t)}{\hbar}\right)\right] + \Delta\sigma_z$$

$$\mathcal{H}_{\mathrm{F},\xi}(\boldsymbol{k}) \simeq \mathcal{H}_{0,\xi}(\boldsymbol{k}) + \frac{[\mathcal{H}_{-1,\xi}, \mathcal{H}_{+1,\xi}]}{\hbar\omega}$$

$$\mathcal{H}_{m,\xi}(\boldsymbol{k}) = \frac{1}{T}\int_0^T dt e^{im\omega t}\mathcal{H}_\xi(\boldsymbol{k}, t)$$

3. Results and Discussion：

衬底和光照竞争下系统的动力学能隙和相图

$$\mathcal{H}_{\mathrm{F},\xi}(\boldsymbol{k}) = \mathcal{H}_{0,\xi}(\boldsymbol{k}) + \xi F_\eta(A)\sigma_z + \Delta\sigma_z \qquad F_\eta(\omega) = \eta(eAv_{\mathrm{F}})^2/\hbar\omega$$

$$= \begin{pmatrix} \Delta + \xi F_\eta(A) & \hbar v_{\mathrm{F}}(k_x - i\xi k_y) \\ \hbar v_{\mathrm{F}}(k_x + i\xi k_y) & -\Delta - \xi F_\eta(A) \end{pmatrix}$$

$$E_\xi(\boldsymbol{k}) = \lambda\sqrt{(\Delta + \xi F_\eta)^2 + (\hbar v_{\mathrm{F}} k)^2} \qquad E_{\xi,\mathrm{g}} = 2|\Delta + \xi F_\eta(\omega)|$$

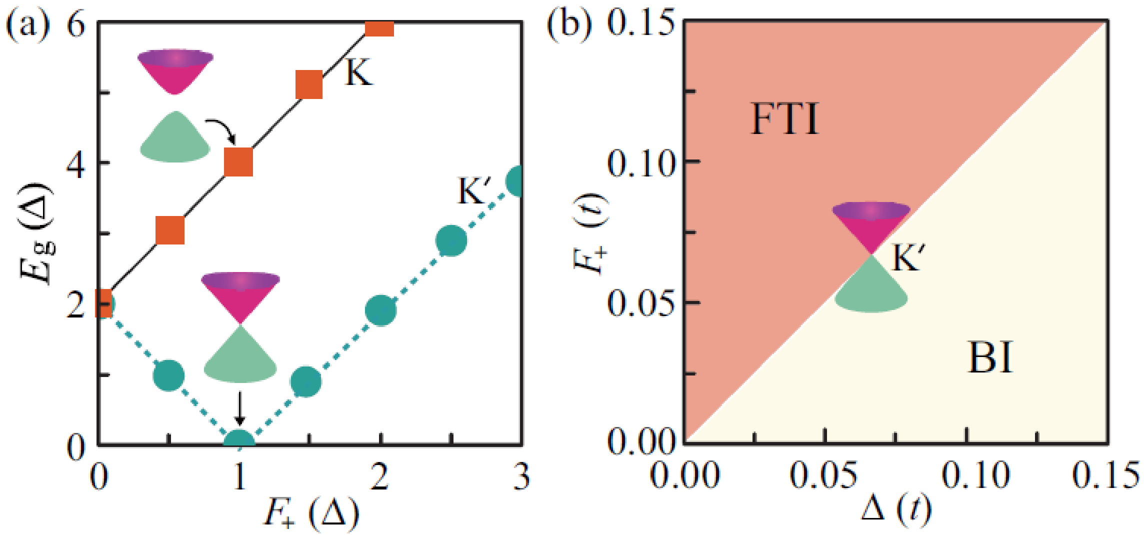

$$I = (eA\omega)^2/(8\pi\alpha)$$

3. Results and Discussion：

紧束缚计算的 Berry 曲率和能带

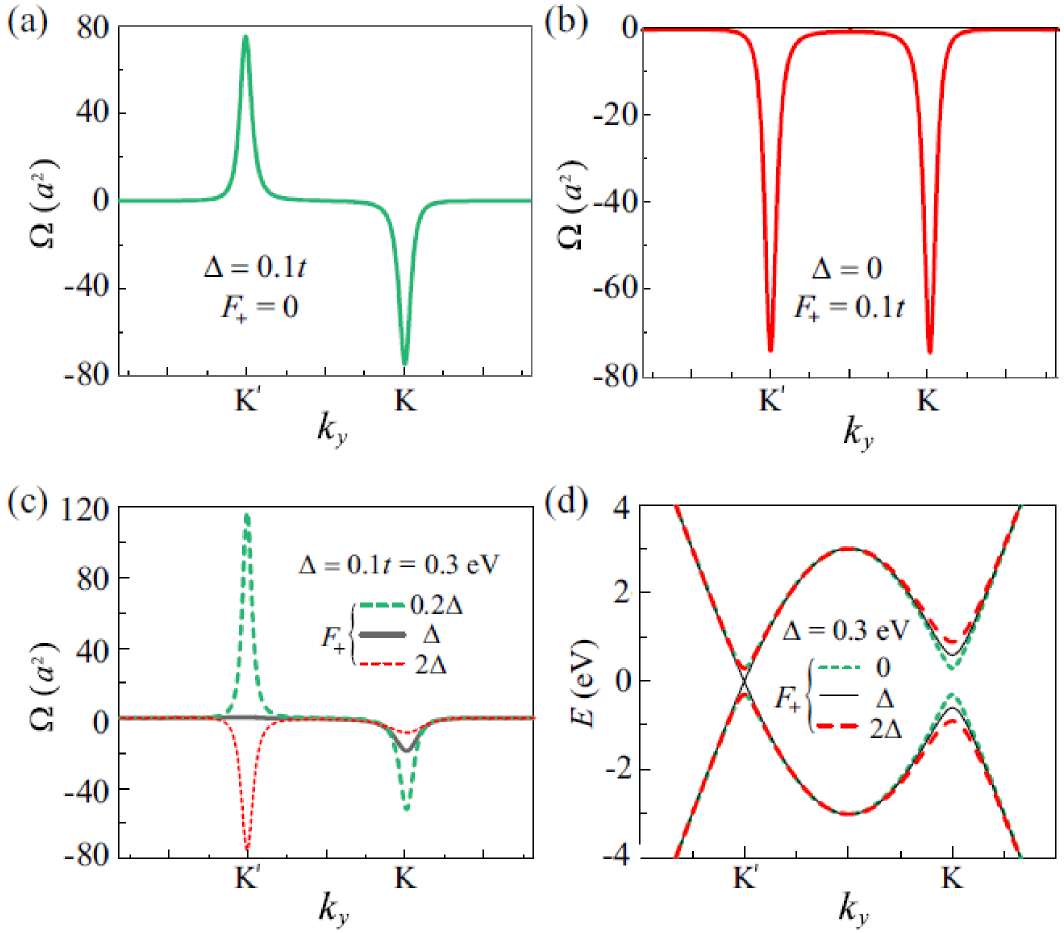

$$\Omega_-(\boldsymbol{k}) = -\frac{(\hbar v_F)^2(\xi\,\Delta + F_\eta)}{2[(\Delta + \xi\,F_\eta)^2 + (\hbar v_F k)^2]^{3/2}}$$

$$\Omega_+(\boldsymbol{k}) = -\Omega_-(\boldsymbol{k})$$

Floquet Chern 数

$$\mathcal{C}_F = \int_{FBZ} \frac{d^2\boldsymbol{k}}{2\pi}\Omega_-(\boldsymbol{k})$$

$=0, \pm 1$

(a), (b) 光照和衬底仅有一个作用存在；(c), (d) 光照和衬底两个作用并存及竞争

3. Results and Discussion：

能带绝缘体相 (BI) 和 Floquet 拓扑绝缘体相 (FTI)

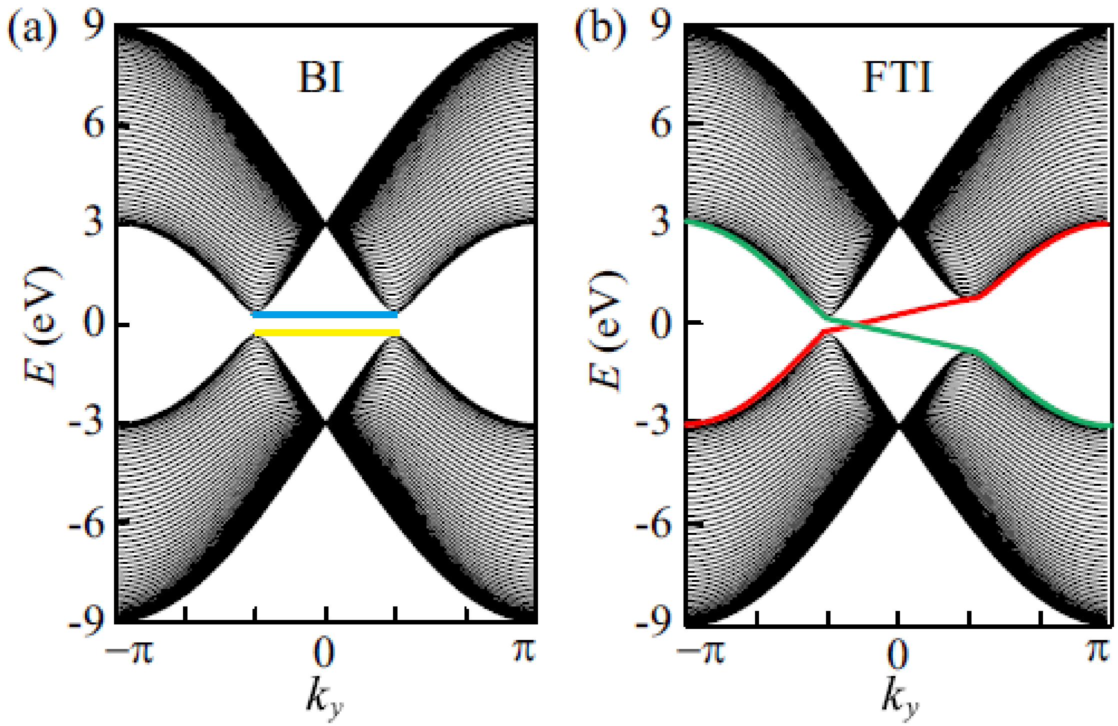

Band structure of a zigzag edged graphene nanoribbon with width 10 nm. (a) $F_+=0$, $\Delta=0.1t$; (b) $F_+=0.15t$, $\Delta=0.1t$.

3. Results and Discussion：

应用1 光传感 np 结

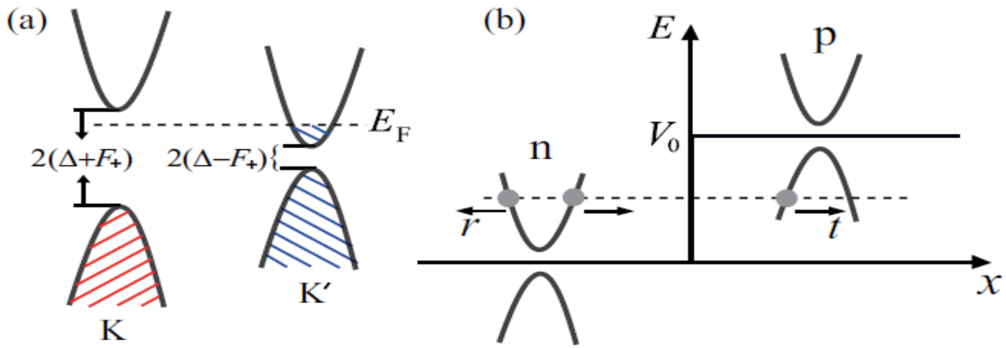

谷内隧穿

谷间隧穿

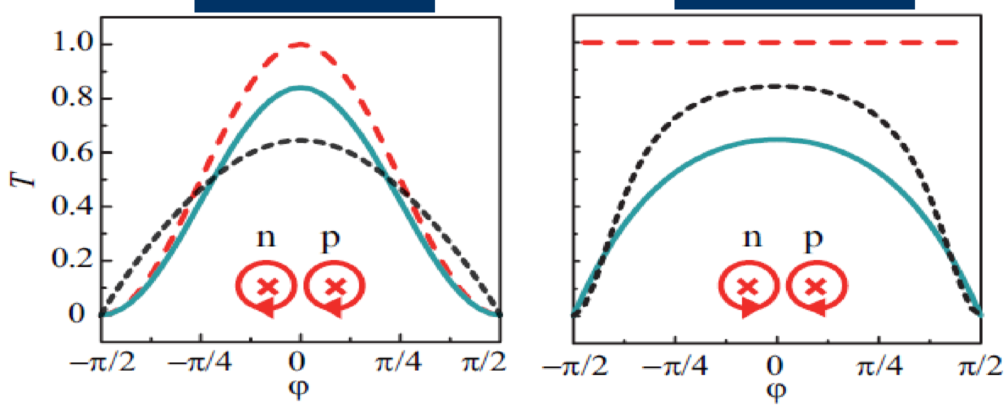

[0, 0.5] [0.2, 0.5] [0.2, 0.25]

$[(\Delta - F_+)/V_0, E/V_0]$

Landauer-Büttiker formula

$$G = G_0 \int_0^{\pi/2} d\varphi T(\varphi) \cos\varphi$$

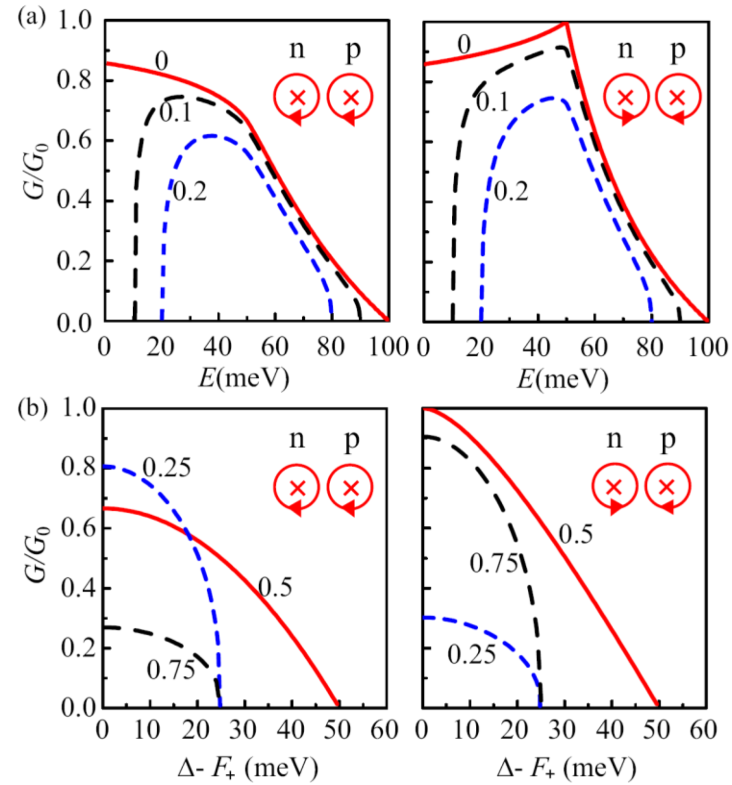

光控谷间隧穿可探测信号更强

3. Results and Discussion：

应用2 光控拓扑场效应晶体管

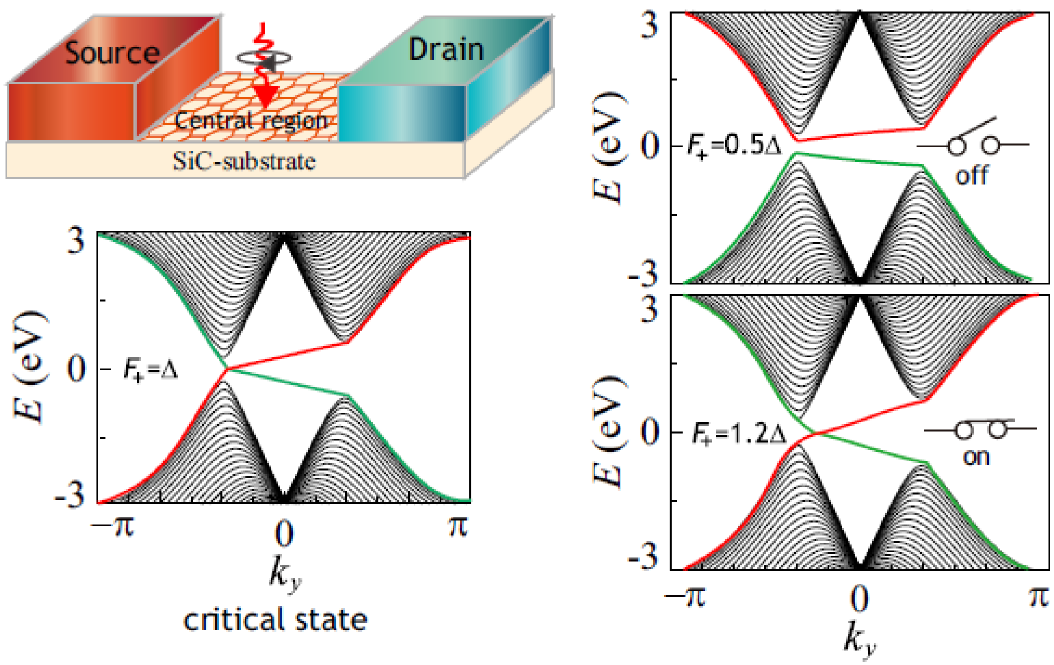

控制光强可以控制晶体管的开关

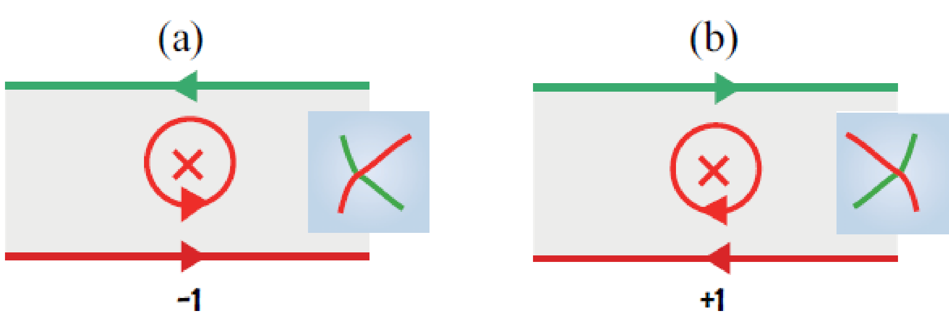

反转光的偏振方向可以反转边模螺旋性

3. Results and Discussion：

应用3 光调节反常热磁效应

The same setup for a graphene monolayer, irradiated by an off-resonance circularly polarized light, on a SiC substrate

$$E(\sigma_z, \tau_z) = (\Delta + \tau_z \Delta_\omega)\sigma_z$$

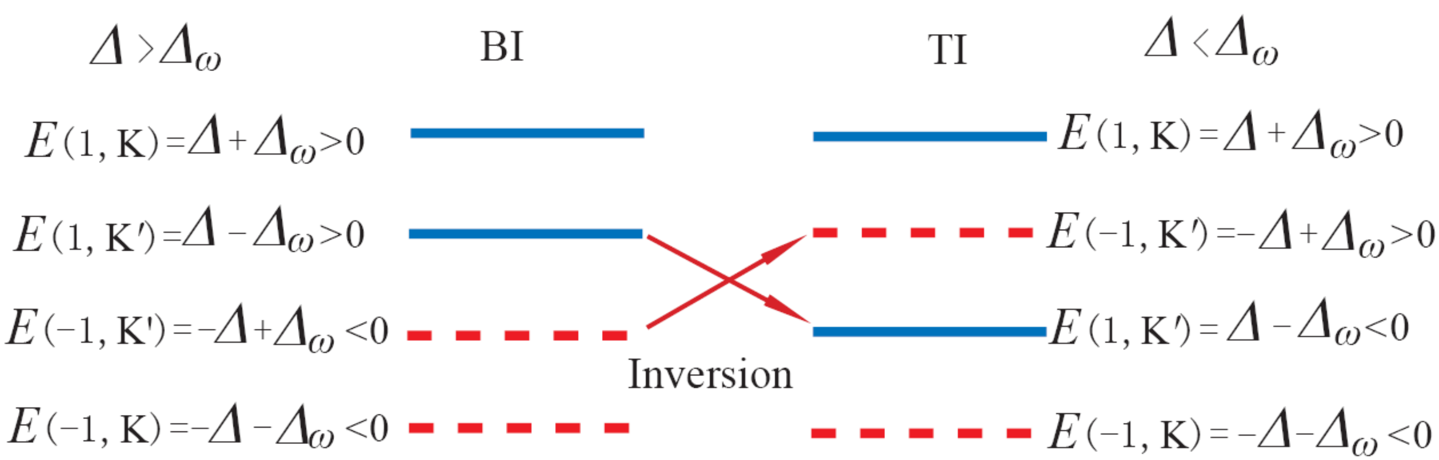

Band inversion. The blue solid (red dashed) lines represent conduction (valence) band in band insulating phase.

Nernst coefficient

$$\alpha_{xy}^{\tau_z} = \frac{2e}{\hbar T}\sum_n \int \frac{d\boldsymbol{k}}{(2\pi)^2}\Omega_n^{\tau_z}[(E_n - E_{\mathrm{F}})f + k_{\mathrm{B}}T\ln(1+e^{-\frac{E_n-E_{\mathrm{F}}}{k_{\mathrm{B}}T}})]$$

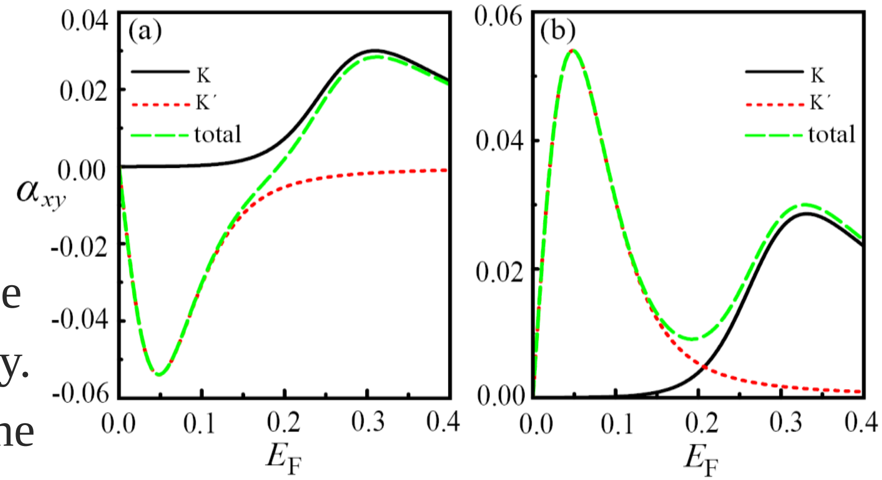

Valley-dependent Nernst coefficient and the total Nernst coefficient versus Fermi energy. (a) In the BI phase (Δ_ω = 0.12 eV); (b) in the TI phase (Δ_ω = 0.14 eV).

$$\alpha_{xy}^{\tau_z} = \frac{\pi^2}{3}\frac{k_{\mathrm{B}}^2 Te}{h}\frac{\tau_z\Delta+\Delta_\omega}{E_{\mathrm{F}}^2}$$

Ettingshausen coefficient

$$\kappa_{xy}^{\tau_z} = T\alpha_{xy}^{\tau_z} = \frac{\pi^2}{3}\frac{k_{\mathrm{B}}^2 T^2 e}{h}\frac{\tau_z\Delta+\Delta_\omega}{E_{\mathrm{F}}^2}$$

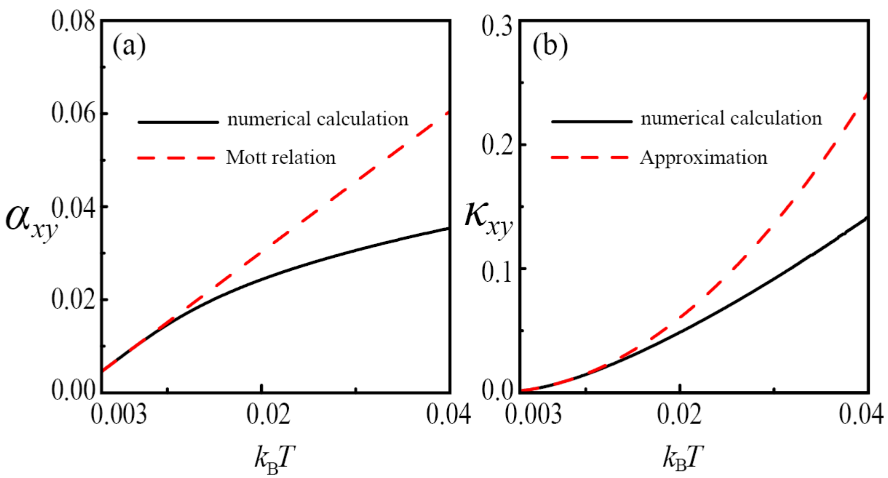

Total Nernst coefficient (a) and total Ettingshausen coefficient (b) versus $k_{\mathrm{B}}T$ at the topological phase transition point with E_{F} = 0.3 eV.

Nernst-Ettingshausen Figure of merit

$$ZT = \frac{\alpha_{xy}^2 T}{\sigma\lambda} = \frac{2\pi\Delta_\omega^2 k_B^2 T^2 h}{3\tau(\Delta_\omega E_{\mathrm{F}}^4 + 2E_{\mathrm{F}}^5)}$$

4. Summary: Some conclusions

考虑衬底和圆偏振光共同作用下的碳单层，利用紧束缚近似 + Floquet 理论，

1) 得到了光照和衬底子格势竞争下的动力学能隙和相图;
2) 证明了外加光照需要达到阈值才能实现 Floquet 拓扑相，相界上，能带在一个谷上是无能隙的 Dirac 锥，而在另一个谷上存在能隙;
3) 普通能带绝缘体相中，靠近 Fermi 能的位置只有一个谷提供电子，通过反转光的偏振方向就可以实现两个谷之间性能的转换;
4) 提出了应用性的电子学装置，即光传感 np 结和光控拓扑型场效应管，以及光调节反常热磁效应

六. 结束语

Graphene-Like Two-Dimensional Materials

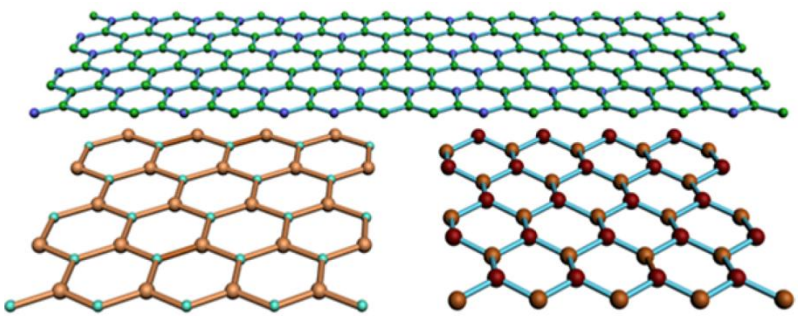

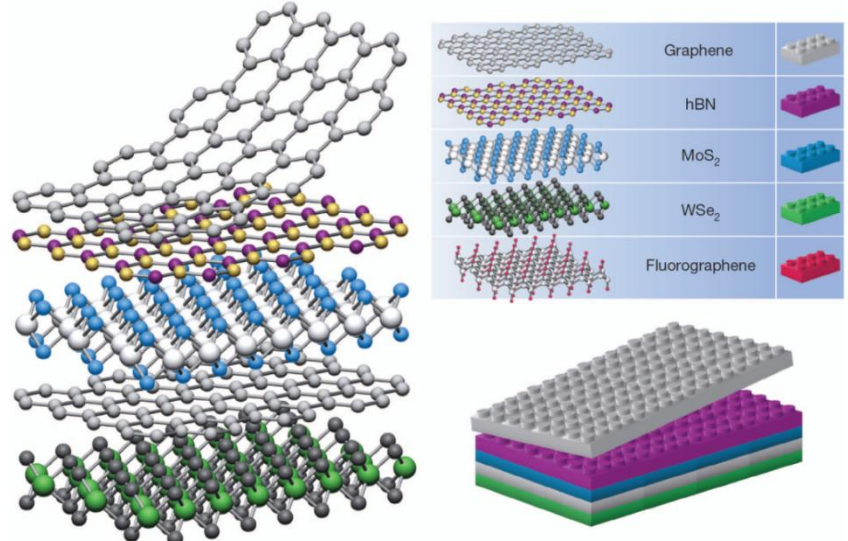

Van der Waals heterostructures

A. K. Geim & I. V. Grigorieva, Nature 499, 419 (2013).

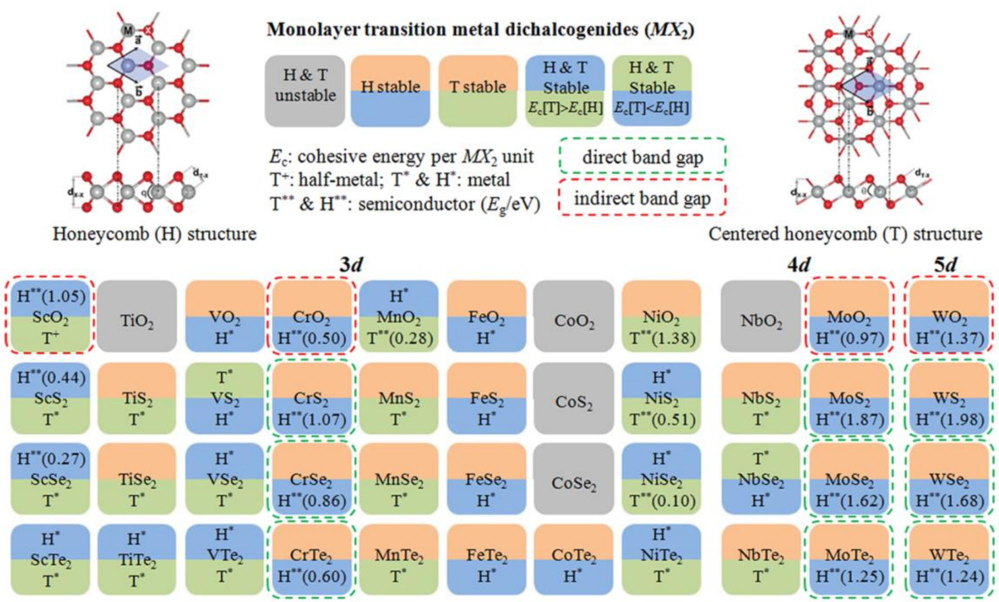

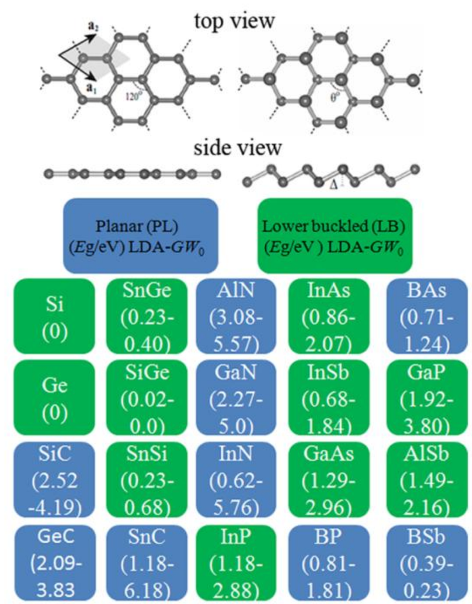

M. Xu, T. Liang, M. Shi, and H. Chen, Chem. Rev. 113, 3766 (2013).

Transport through graphene quantumdots

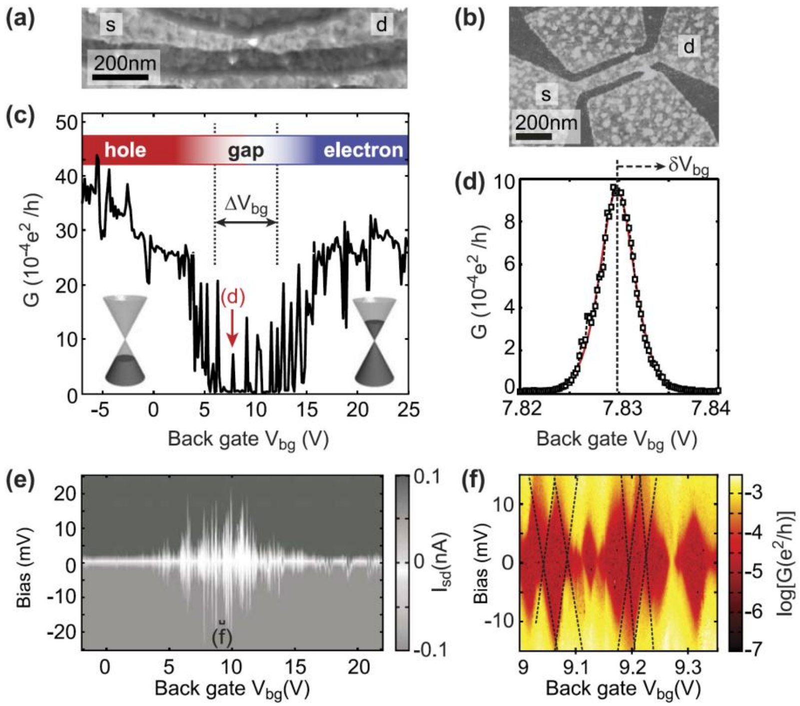

J. Guttinger et al., Rep. Prog. Phys. 75, 126502 (2012).

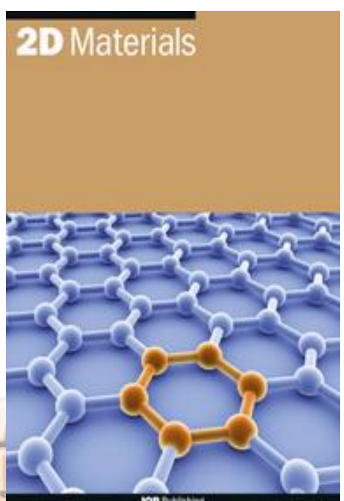

Vladimir Fal'ko
Editor-in-Chief
2D Materials

Two-dimensional flexible nanoelectronics

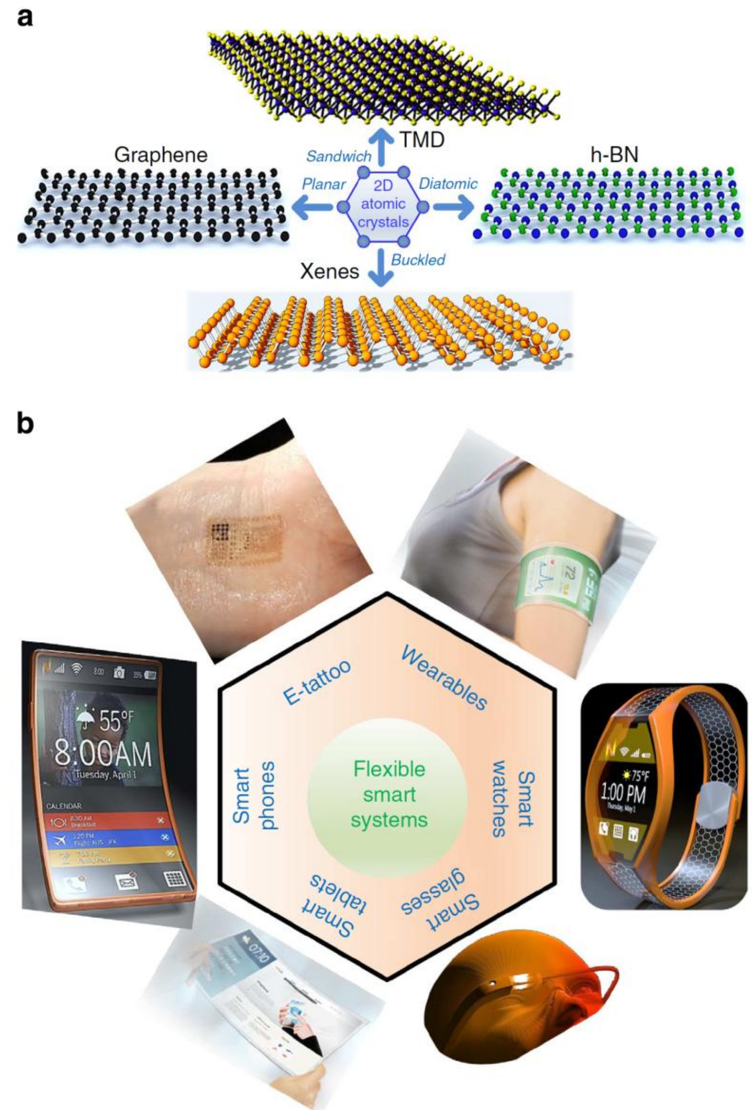

Akinwand, Petrone & Hone, Nat. Commun. 5, 5678 (2014).

翟学超, 戚凤华, 许亚芳, 周兴飞, 金国钧, 物理学进展 35, 1 (2015).

NATURE NANOTECHNOLOGY | VOL 10 | MAY 2015 | www.nature.com/naturenanotechnology

editorial

Graphene opens up to new applications

Effective separation membranes could be created by etching nanometre-sized pores in two-dimensional materials.

The explosion of research interest in two-dimensional materials such as graphene and molybdenum disulphide has, to a large extent, been dominated by their physics, and in turn the exploitation of their electronic and optical properties. Researchers have, of course, also explored the chemical and mechanical properties of these materials — and sought applications that principally utilize these attributes — but the results have, arguably, received less attention. One intriguing line of research in this regard is the use of graphene as a nanoporous separation membrane. Here, through a combination of sophisticated fabrication and characterization techniques, unique membranes could be developed for use in critical applications such as gas separation, water purification, and desalination.

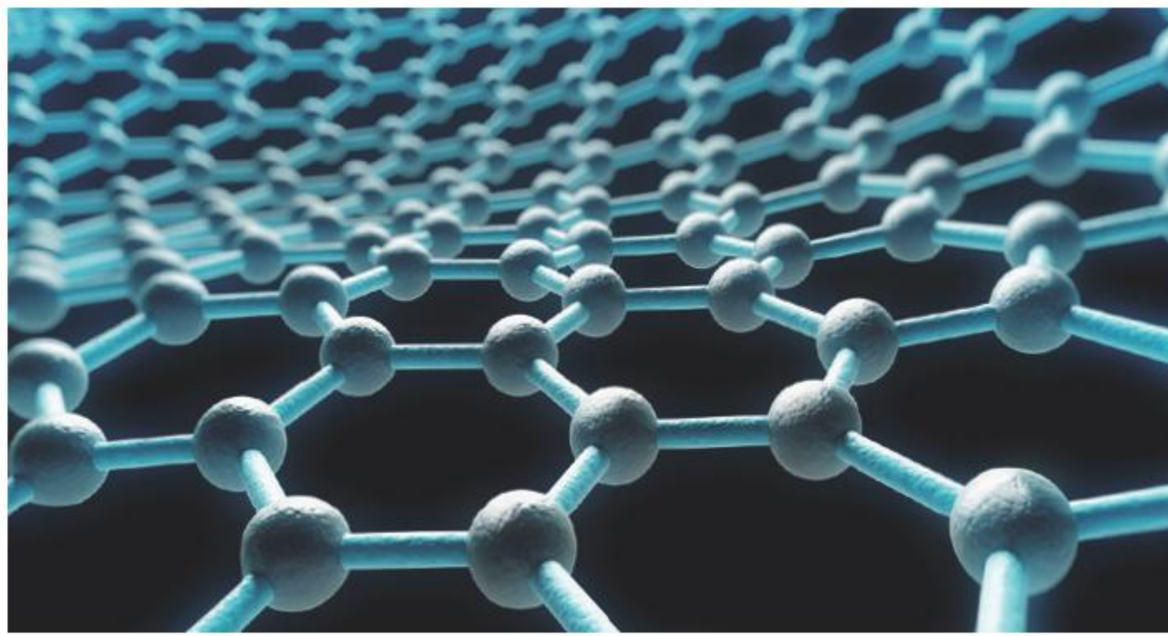

reported that subnanometre pores can be formed over macroscopic areas of graphene

encouraging illustration of the potential of atomically thick membranes.

NATURE MATERIALS | VOL 14 | APRIL 2015 | www.nature.com/naturematerials

editorial

Physics gets its hands dirty

Is condensed-matter physics becoming more materials-oriented? Or is this just a new wrinkle in an old tradition?

Thanks!

国家基础研究项目 (**2011CB922102**), 江苏省优势学科建设工程 (PAPD)，和国家自然科学基金 (11074108) 的支持